AFRL-AFOSR-UK-TR-2015-0024

CHARACTERIZATION OF IONOSPHERE WAVEGUIDE PROPAGATION BY MONITORING HAARP HF TRANSMISSIONS IN ANTARCTICA

***Yuri M. Yampolski**

SCIENCE AND TECHNOLOGY CENTER IN UKRAINE
METALISTIV 7A, KYIV, UKRAINE

***INSTITUTE OF RADIO ASTRONOMY**
NATIONAL ACADEMY OF SCIENCES OF UKRAINE
4, CHERVONOPRAPORNA SR, KHARKOV 61002 UKRAINE

EOARD STCU P-524/STCU 10-8002

Report Date: April 2015

Final Report from 1 January 2012 to 31 December 2014

Air Force Research Laboratory
Air Force Office of Scientific Research
European Office of Aerospace Research and Development
Unit 4515, APO AE 09421-4515

REPORT DOCUMENTATION PAGE

Form Approved OMB No. 0704-0188

1. REPORT DATE *(DD-MM-YYYY)*	2. REPORT TYPE	3. DATES COVERED *(From – To)*
17 April 2015	Final Report	1 January 2012 – 31 December 2014

4. TITLE AND SUBTITLE

CHARACTERIZATION OF IONOSPHERE WAVEGUIDE PROPAGATION BY MONITORING HAARP HF TRANSMISSIONS IN ANTARCTICA

5a. CONTRACT NUMBER

STCU P-524

5b. GRANT NUMBER

STCU 10-8002

5c. PROGRAM ELEMENT NUMBER

61102F

6. AUTHOR(S)

***Yuri M. Yampolski**

5d. PROJECT NUMBER

5d. TASK NUMBER

5e. WORK UNIT NUMBER

7. PERFORMING ORGANIZATION NAME(S) AND ADDRESS(ES)

SCIENCE AND TECHNOLOGY CENTER IN UKRAINE
METALISTIV 7A, KYIV, UKRAINE

*INSTITUTE OF RADIO ASTRONOMY
NATIONAL ACADEMY OF SCIENCES OF UKRAINE
4, CHERVONOPRAPORNA SR, KHARKOV 61002 UKRAINE

8. PERFORMING ORGANIZATION REPORT NUMBER

N/A

9. SPONSORING/MONITORING AGENCY NAME(S) AND ADDRESS(ES)

EOARD
Unit 4515
APO AE 09421-4515

10. SPONSOR/MONITOR'S ACRONYM(S)

AFRL/AFOSR/IOE (EOARD)

11. SPONSOR/MONITOR'S REPORT NUMBER(S)

AFRL-AFOSR-UK-TR-2015-0024

12. DISTRIBUTION/AVAILABILITY STATEMENT

Distribution A: Approved for public release; distribution is unlimited.

13. SUPPLEMENTARY NOTES

14. ABSTRACT

The Project was aimed at experimentally investigating the possibility of exciting the ionospheric interlayer duct channel using powerful radiation from the heaters HAARP (Alaska, USA) and EISCAT (Tromsø, Norway), as well as from HF broadcasting stations RWM (Moscow, Russia) and CHU (Ottawa, Canada). Major attention was paid to analyzing the possibility of exciting the interlayer ionospheric waveguide which support super-long range HF propagation with a small amount of attenuation. To monitor the radiation, a compact-size receiving complex was developed which is capable of measuring the signal intensity and spectral characteristics in an off-line automatic mode. Two facilities have been constructed in the course of the Project. One was deployed in Ukraine at the Low-frequency Observatory of the IRA NASU (Martova village, Kharkov region) in 2012, while another was installed at the Ukrainian Antarctic station "Akademik Vernadsky" in the Antarctic in 2013. In all, about 100 hours were spent observing the radiation from the heaters (primarily EISCAT) and more than 3000 hours monitoring signals from broadcast radios. In a number of cases the signal strengthening was detected for the super-long range radio links (Alaska-Antarctica and Northern Scandinavia-Antarctica) which effect can be regarded as a result of the waveguide propagation. A pioneering feature of the developed theoretical model is accounting for the regular ionospheric refraction. The aspect-sensitive contours in the ionosphere and on the Earth's surface have been calculated for all the transmitting and receiving sites for the current ionospheric conditions. A software package was developed for the remote control of the receiving complexes and visual representation of the measurement results in real-time over the internet. The most productive experiments were performed during the BRIOCHE heating campaign in June 2014. The detailed description of this campaign is included in Chapter 4 of the Final Report. The results obtained during the Project were published in fours scientific papers and reported at several international meetings in the USA, Puerto-Rico and Ukraine.

15. SUBJECT TERMS

EOARD, Materials, mictrostructural characterization, high temperature

16. SECURITY CLASSIFICATION OF:			17. LIMITATION OF ABSTRACT	18, NUMBER OF PAGES	19a. NAME OF RESPONSIBLE PERSON
a. REPORT	b. ABSTRACT	c. THIS PAGE			homas R. Caudill
UNCLAS	UNCLAS	UNCLAS	SAR	33	19b. TELEPHONE NUMBER *(Include area code)* +44 (0)1895 616186

Science and Technology Center in Ukraine

Partner Project № 524

CHARACTERIZATION OF IONOSPHERE WAVEGUIDE PROPAGATION BY MONITORING HAARP HF TRANSMISSIONS IN ANTARCTICA

Final report (Full Form)

Director,
Institute of Radio Astronomy,
National Academy of Sciences
of Ukraine

Professor
Leonid Lytvynenko

Manager, Project P-524

Professor
Yuri Yampolski

Kharkiv-2014

CHARACTERIZATION OF IONOSPHERE WAVEGUIDE PROPAGATION BY MONITORING HAARP HF TRANSMISSIONS IN ANTARCTICA

Project manager: Yuri M. Yampolski

1. Introduction

The nonmonotonic run of the height profile of the ionospheric electron density associated with the multilayered structure of the ionosphere creates preconditions for formation of interlayer duct channels. These natural structures are capable of supporting the radio wave energy transfer to long distances (thousands and tens of thousands of kilometers) with low losses. The valley between the E- and F-layer maxima seems to be energetically optimal from this point of view. The characteristic boundaries of such a duct vary between 120 and 150 km on the bottom and from 200 to 250 km on the top, depending on the wave frequency and geophysical conditions (geographic coordinates, sunlit conditions, season, geomagnetic activity etc.). At HF waves the duct represents a multimode waveguiding structure since the wavelength λ is much shorter than the waveguide size h. The ionospheric duct is characterized by a small amount of losses owing to the comparatively low collision frequency of electrons ν_e whose value is two or three orders of magnitude lower than at heights of the main absorbing D-region of the ionosphere. This is a reason why the attenuation rate of HF signals in the interlayer duct is dozen of times smaller than for ordinary multi-hop propagation paths.

The major problem of using the ionospheric duct in practice is the difficulty of exciting the channel from the Earth's surface and extracting energy for a ground-based consumer. The reason is that the E-layer plays the role of a barrier which shades the above layers from the HF emission radiated by a ground-based transmitter at frequencies below the critical frequency of the E-region. The signal input in and extraction from the interlayer duct channel is possible only in the presence of considerable horizontal gradients of the electron density or intense scattering irregularities. For the known geometry of the propagation path it is possible to select the most favorable conditions for feeding-in (feeding-out) the waveguide proceeding from the variable sunlit conditions and hence, the predictable horizontal gradients of the electron density distribution. Such conditions can be mainly realized for rather long-range radio paths of meridional orientation close to the sunrise or sunset at ionospheric heights. Pointing the transmitting and receiving antennas in certain oblique directions and changing the radiation frequency it is possible to arrange a scenario where the bottom wall of the waveguide (E-region) would exist along the entire radio path, except the ascending (descending) section of the trajectory in a given vicinity of the transmitting (receiving) site. Such situations are well known to occur in practice of radio broadcast and communication when the solar terminator passes almost simultaneously the transmitter and receiver sites. This can be accompanied by a considerable increase in the received signal level.

The effects of the energy input and output owing to radio wave scattering by intense natural ionospheric irregularities are of unpredictable character. Their appearance is determined by sporadic factors and depends, specifically, on the enhanced turbulization of the ionopsheric plasma produced by various kinds of geophysical perturbations. Especially frequent such effect are at high latitudes which are to a greater extent subjected to the influence of magnetic and corpuscular perturbations stimulated by solar wind flux variations. It is evident that predictable input (output) of the useful signal into (from) the duct using the effects of scattering by natural structures of the kind is impossible. In addition, the life time of the necessary irregularities is unpredictable as well and varied, as a rule, from a few seconds to dozen of minutes.

Extra chances for exciting the interlayer duct can be provided by active experiments on ionosphere modification which allow controlling the space and time structure of the ionospheric turbulence. Primarily this concerns the ionospheric heating by the powerful HF emission from a ground-based transmitter. As is known, the major result of the nonlinear interaction between the incident wave and ionospheric plasma is generation of the artificial ionospheric turbulence (AIT), whose space-and-time spectrum can be controlled using special heating regimes. As a rule, the horizontal scale of the AIT-containing region is determined by the antenna pattern width of the heater and can be estimated to lie between 100 and 200 km, depending on the modified region altitude and the heating frequency. It is evident that the stimulated irregularities are of a stochastic character, however a number of their morphological features are a priori known. These are the location; times of appearance, existence and relaxation; spatial anisotropy due to the magnetized plasma; external scale-size of the turbulence; and even spatial spectrum in the case of special heating modes. With allowance for such deterministic features, the AIT can be used for exciting the interlayer channel. The output of the signal from the waveguide can be provided by horizontal gradients produced by the solar terminator near the receive site of a super long-range path.

A pioneering feature of the developed theoretical model is the account of the regular ionospheric refraction. The aspect-sensitive contours in the ionosphere and on the Earth's surface have been calculated for all the transmitting and receiving sites for the current ionospheric conditions. During the measurement campaigns with the use of radiations from the powerful heaters two other effects have been occasionally revealed, which are the combination (Brillouin) signal scattering by the artificially stimulated plasma turbulence and excitation of the second harmonic of the powerful radiation in the HF-modified ionosphere. As planned, a software package has been developed for the remote control of the receiving complexes and visual representation of the measurement results in real-time through the internet.

Taking into account that the most powerful heaters HAARP and EISCAT are located close to the northern polar regions (Alaska and Northern Scandinavia, respectively), the most promising position to observe the waveguide propagation effects of HF signals to super-long distances seems to be Antarctic. An additional reason in favor of this region is the "purity" of the electromagnetic climate because of the absence of intense man-caused interference and local thunderstorm activity. The first successful experiments on registration of signals from a powerful heating facility in Antarctic region were performed by the Institute of Radio Astronomy in 2002. The results suggested that the waveguide propagation can apparently be realized *Zalizovski* et al, [2009]. The probe signal was the proper emission from the EISCAT heater which was scattered by AIT inside the interlayer duct. The receiving site was deployed in Antarctica at the Ukrainian base "Akademik Vernadsky". In a number of cases, along with the usual quite stable component associated with multi-hop propagation through the sidelobes of the heater antenna, rather strong signals were reliably detected whose spectra allowed suggesting that they were scattered by AIT produced by the heater emission itself. Most frequently the scattered component was observed close to the time of solar terminator passage through the radio path. The effect has been called the "self-scattering" of powerful HF signals by the ionospheric turbulence stimulated by the same signals *Zalizovski* et al, [2009]. However these were trial episodic experiments, which have not allowed investigating in detail various mechanisms of radio signal propagation.

The present Project was aimed at comprehensive studying the super long-range propagation mechanisms through monitoring the HAARP and EISCAT heaters emissions with the use of a specially constructed automated internet-controllable HF receiver. Possible receiving site should been deployed in Antarctica at the Ukrainian Antarctic station (UAS) "Akademik Vernadsky" (65^0 15' S, 64^0 16' W). The distances between HARRP and EISCAT heaters and Antarctic position are 15 600 km and 16 100 km correspondently.

2. Mobile HF receiving system

For the Stage 1 of the Project the mobile HF receiving complex was created and installed at the Low Frequency Observatory of IRA NASU(LFO) for tests and continuous measurements. The receiving facility has been budett around the WR-G313i digital receiver of the WiNRADiO communications (Australia, www.winradio.com.au), which has shown good performance. The receiver should be designed as a PCI card to be inserted into and extender slot of the PC mainboard. A general view of the receiver is shown in Fig. 2.1.

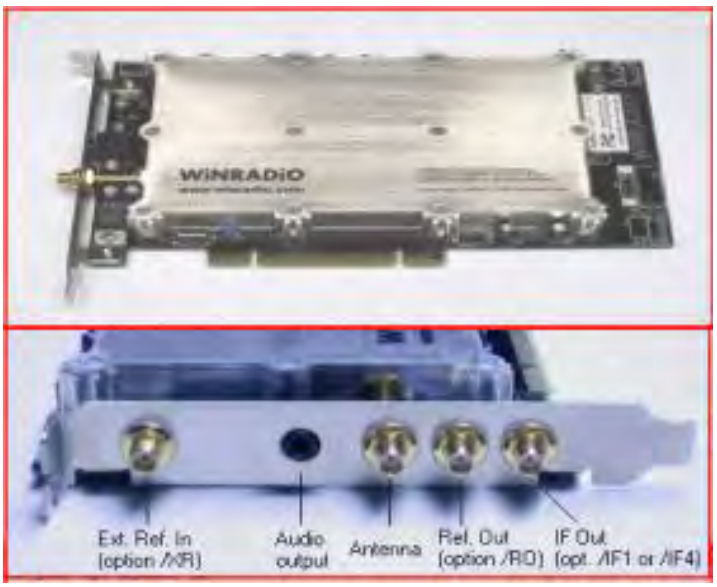

Fig. 2.1. General view of the WR-G313i receiver

The basic performance specifications of the receiver are listed in Table 2.1.

Table 2.1 Performance specifications of the WR-G313i receiver

Receiver type	Superheterodyne receiver with a signal processor
Frequency range	9 kHz to- 30 MHz
Frequency adjustment accuracy	1 Hz
Dynamic range	95 dB (112 dB with an input attenuator)
Sensitivity	0.05 μV
Frequency band	Variable between 1 and 1500 Hz with 1 Hz step
Intermediate frequencies	IF1: 45 MHz IF2: 16 kHz (adjustable between 12 and 22 kHz)
IF1 bandpass filter	15 kHz crystal filter
Antenna input	50 Ω
Form factor	2/3 PCI card, PCI 2.2 compatible
Weight	330 g

To provide for the required frequency instability of the receiver ΔF/F no worse than 10^{-8}, a temperature-compensated compact-size crystal oscillator developed at the IRA NASU will be used. The oscillator is designed as a standard 5" PC device to be inserted in a computer (Fig. 2.2).

Fig. 2.2. Compact-size temperature-compensated crystal oscillator

An active loop antenna developed at the IRA NASU is to be used as to receive the signals. The antenna provides for a high sensitivity within the frequency range 3 to 15 MHz. The design of the loop antenna with the pre-amplifier is shown in Fig. 2.3

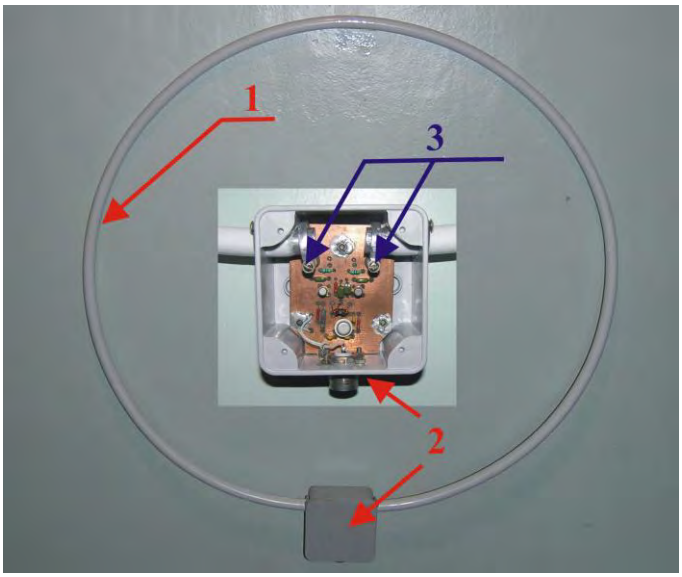

Fig. 2.3. Active loop antenna (1,) broadband pre-amplifier (2), and fixing parts (3)

A special software package developed at the IRA NASU allows remotely controlling the receiver and real-time data reading through the Internet. To detect the useful signal, Doppler spectra of the received emission are computed within a narrow frequency range (about 100 Hz) with a spectral resolution ~0.1 Hz. Fig. 2.4 shows the user window interface intended for frequency tuning of the

receiver through the Internet and visual representation of the current measurement data in the form of the signal envelope (a) and instantaneous (b) and dynamic (c) spectra.

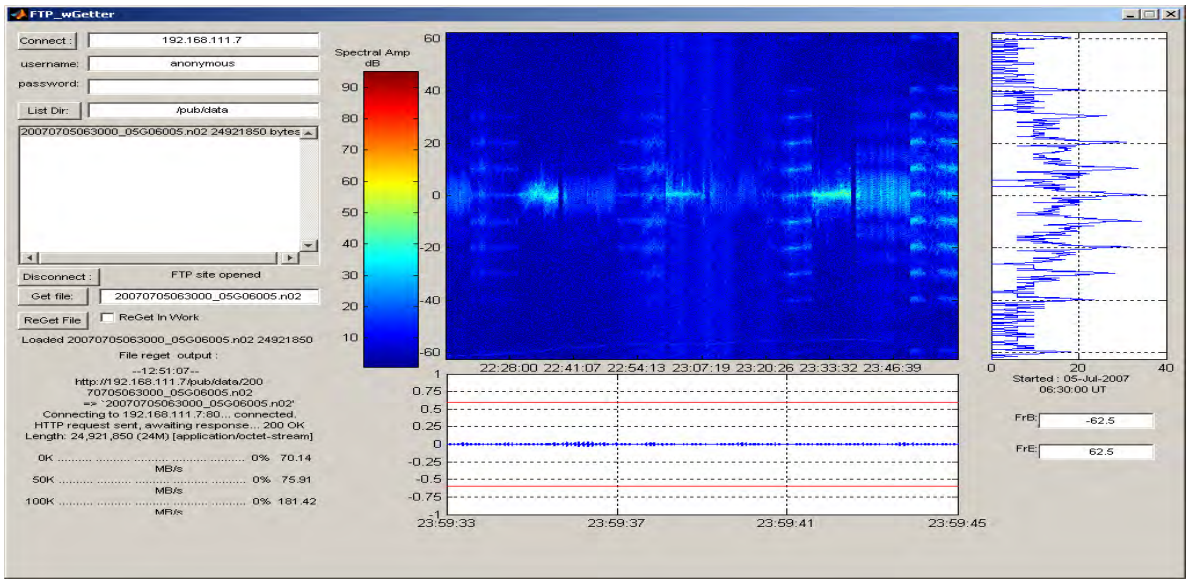

Fig. 2.4. User window interface of the receiver control and data reading

A general view of the receiver with a control computer is shown in Fig. 2.5.

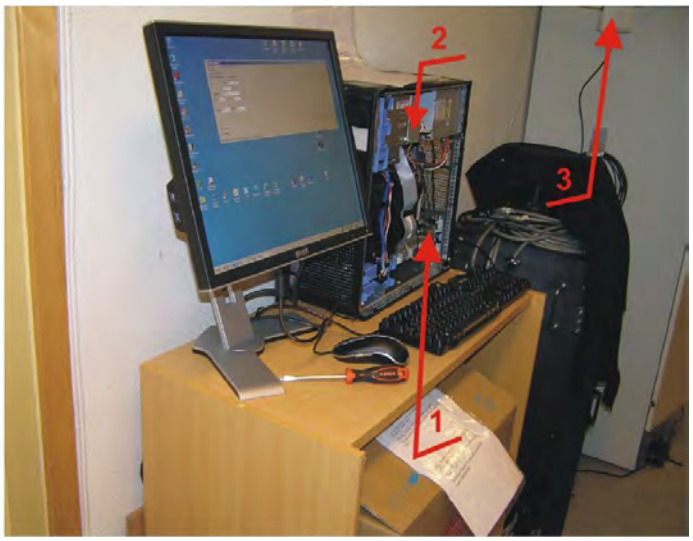

Fig. 2.5. General view of the receiving complex: 1 - WR-G313i receiver, 2 - reference oscillator, and 3 – antenna cables

The similar receiving complex was created for installation in Antarctica on the Stage 2 of the Project. On March 2013 this system deployed at the Ukrainian Antarctic station "Akademik Vernadsky" and operates continuously registering now emissions from HF broadcasting stations and signals from the HAARP and EISCAT heaters.

3. HF wave scattering by field-aligned plasma irregularities considering refraction in the ionosphere

The effect of ionospheric refraction on the scattering of high frequency (HF) signals by random field-aligned irregularities in the upper ionosphere was analyzed in a frame of a theoretical part of the Project. The possibility of excitation of the ionospheric interlayer waveguide by the aspect-sensitive scattered HF signals is analyzed in detail for the specific conditions of the HF heating experiments. Aspect-sensitive scattering of high-frequency (HF) (3-30 MHz) and very high-frequency (VHF) (30-300 MHz) waves by field-aligned irregularities of the ionospheric plasma are widely used for diagnostics of turbulent processes in the near-Earth plasma of both natural [Lyon, 1965; Bourdillon et al.,1995; Bezrodny et al., 1997] and artificial [Djuth et al., 2006; Hysell, 2008; Yampolski et al., 1997; Koloskov et al., 2002] origins. Theoretical premises for this method of diagnosing the inhomogeneous structure of the ionosphere were developed within the single-scattering approximation [Rytov et al., 1987]. As a rule, in the relevant studies the condition $\omega^2 >> \omega_{cr}^2 >> \omega_H^2$ is assumed, where ω is the cyclic frequency of the sounding signal, ω_{cr} is the critical frequency of the ionospheric layer (i.e., the maximum plasma frequency $\omega_{p\max}$), and ω_H the electron gyrofrequency. This assumption makes it possible to ignore the effects of the regular ionospheric refraction and background geomagnetic field. Consequently, the wave trajectories are approximated by straight lines, and ionospheric plasma is assumed isotropic.

However, to be precise, in order to ignore the effects of refraction stronger conditions have to be satisfied, which can be derived as follows. The equation for the incident ray trajectory in a plane-stratified ionosphere can be written as [Kravtsov and Orlov, 1990]:

$$x(z) = \sin\theta_0 \int_{z_0}^{z} \frac{dz}{\sqrt{\cos^2\theta_0 - \omega_p^2(z)/\omega^2}},$$

where θ_0 is the angle of incidence at the lower boundary of the ionospheric layer, z_0, counted from the vertical. Obviously, in order for a wave to penetrate through the ionosphere (with no reflection point at which the ray curvature would be the greatest), the following condition must be satisfied: $\omega > \omega_{cr}/\cos\theta_0$; while in order to approximate the ray trajectories by straight lines, an even stronger condition should hold: $\omega >> \omega_{cr}/\cos\theta_0$. Here is an example from practice. During most of the experiments on HF signal scattering from artificial ionospheric turbulence (AIT) produced by the Sura HF heater (Nizhny Novgorod, Russia) [Yampolski et al., 1997; Myasnikov et al., 2001; Koloskov et al., 2002], the geometry was such that $\theta_0 \approx 70°$ (for the probe signal) and $f_{cr} = \omega_{cr}/(2\pi) \geq 4.5$ MHz. Therefore, in order to be able to ignore the effects of refraction, the probe signal frequency should be much higher than ~13 MHz, which was rarely the case. Therefore, for correct analysis and interpretation of experiments of the kind, the refraction effects need be taken into account.

It is especially important to account for the ionospheric refraction in analyzing the scattering of powerful HF emissions on the ionospheric irregularities produced by the same radiation. The fact that HF pump wave scatters on ionospheric irregularities is rather trivial and has been observed a long time ago (Belikovich, et al.,1975; Erukhimov et al., 1980). It was not clear, however, whether the scatter signals can travel over the large distances away from the heater, for example, through the ionospheric waveguide. Such effect was apparently first experimentally discovered by Zalizovsky et al. [2009] using the EISCAT HF heater (Tromso, Norway) and was given the name “self-scattering effect”. In their experiment the EISCAT transmission was monitored at three greatly dispersed receiving sites: at the Ukrainian Antarctic

station “Akademik Vernadsky” (UAS); at the Radio Astronomical Observatory of the IRANASU (RAO) near Kharkov, Ukraine; and near Sankt-Petersburg, Russia (SPB). Typically, the received signals contained two characteristic spectral components. One component was a relatively narrow line with insignificant Doppler shift variations characteristic of the sky-wave HF propagation in middle latitudes. The spectrum of the other component was much broader reminiscent of that of a signal scattered at frequencies above the maximum usable frequency (MUF). The broadband (scattered) spectral component exhibited strong frequency fluctuations with amplitude rate occasionally exceeding 10 Hz. However, the most notable observational fact was that the Doppler frequency shifts and intensities of this component varied practically synchronously at all three receive sites with nearly the same oscillation rate. The authors concluded that the observed Doppler shifts of the broadband spectral component were likely induced within a wave trajectory segment that was common to all the propagation paths, i.e., where the HF pump wave travels from the heater to the scattering region with the AIT. Simultaneous observations by the EISCAT incoherent scatter radar showing strong variations in the electron density above the HF heater are supporting the suggested mechanism. However, the exact mechanism of the super long range propagation of the HF heater signals (the EISCAT-UAS propagation distance was ~16,300 km) still has not been determined, and it is quite possible that ionospheric refraction may play an important role since the experiments at the EISCAT location were conducted at frequencies below the critical frequency of the ionosphere ($\omega \le \omega_{cr}$). Galushko et al. [2008] had also observed the self-scattering effect by monitoring the HAARP transmission at several remote sites in the USA, Europe, and Arctic using digital Doppler receivers of the Institute of Radio Astronomy (Kharkov, Ukraine) and Lowell Digisondes.

The aim of the current Project investigation is to develop a general theory for the aspect-sensitive scattering of electromagnetic waves taking into account ionospheric refraction effects on the incident and scattered wave trajectories. We will specifically analyze a possibility of signal channeling in a given direction as a result of such scattering. The work on HF signal trapping in ionospheric waveguides due to scattering was pioneered in 1970’s (e.g., Erukhimov et al., 1975 Gurevich et al., 1975). Our approach, however, is quite different from those studies as we will analyze the range of incidence angles at the lower boundary of the ionosphere responsible for channeling signals in a given direction rather than evaluate a “trapping coefficient” for HF waves. The gyrotropic effects of the ionospheric plasma on the radio wave propagation will be assumed negligibly small. Note that this is quite legitimate first-step approach used in earlier works as well (e.g., Gurevich et al., 1975).

Let a plane monochromatic electromagnetic wave be propagating in a horizontally stratified ionosphere from the lower half-space through the ionospheric layer (see Figure 3.1). The wave is characterized by a frequency ω and wave vector $\vec{k}^{(i)}(0) = \left\{k_x^{(i)}(0), k_y^{(i)}(0), k_z^{(i)}(0)\right\}$. Here $k_x^{(i)}(0) = k_0 \sin\theta_0 \cos\varphi_0$, $k_y^{(i)}(0) = k_0 \sin\theta_0 \sin\varphi_0$ and $k_z^{(i)}(0) = k_0 \cos\theta_0$, where $k_0 = \omega / c$, and angles θ_0 and φ_0 determine the direction of the wave vector at the lower boundary of the ionosphere $z = 0$. The wave frequency ω is assumed to be much higher than the electron gyrofrequency ω_H, i.e. $\omega >> \omega_H$. This makes it possible to treat the ionosphere as an isotropic medium, and to assume the propagating waves to be transversal. In order to avoid any confusion, the following nomenclature will be used in our analysis. The HF waves will be regarded as “incident” and “scattered” with respect to the scattering on the ionospheric irregularities. With respect to the propagation in the ionosphere, the waves will be considered as “direct” and “reflected”.

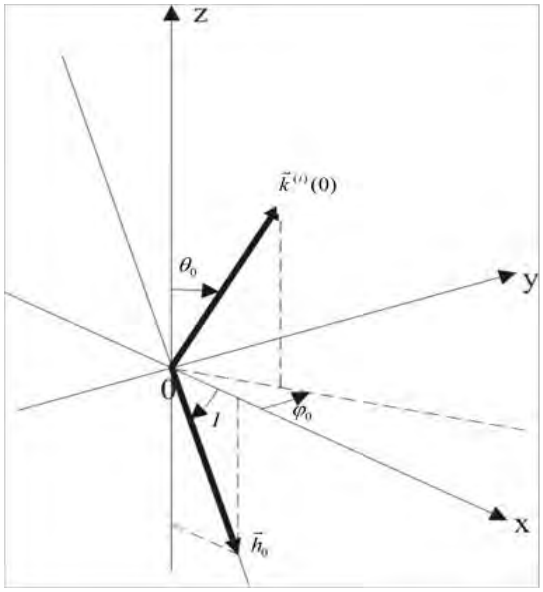

Fig. 3. 1. Coordinate system for the problem. X -axis points toward the geomagnetic north pole. $\vec{h}_0$ vector indicates the direction of the local magnetic field. $\vec{k}^{(i)}(0)$ is the incident wave vector at the lower ionospheric boundary.

The ionosphere will be specified as a plane-stratified collisionless dielectric medium containing random irregularities:

$$\varepsilon(\vec{r},z)=\begin{cases}\varepsilon_0(z)+\delta\varepsilon(\vec{r},z), & z\geq 0;\\ 1, & z<0.\end{cases}$$

Here $\vec{r}=\{x,y\}$ are horizontal coordinates; $\varepsilon_0(z)$ is a regular (i.e., without irregularities) component of the dielectric permittivity of the ionosphere,

$$\varepsilon_0(z)=1-\frac{\omega_p^2(z)}{\omega^2}=1-\frac{4\pi e^2 N_0(z)}{m\omega^2}, \qquad (1)$$

where $N_0(z)$ is a regular electron density profile, and e and m are the electron charge and mass, respectively; and $\delta\varepsilon(\vec{r},z)=\frac{4\pi e^2\delta N(\vec{r},z)}{m\omega^2}$ is a random addition due to electron density fluctuations $\delta N(\vec{r},z)$, characterized by zero mean $<\delta N(\vec{r},z)>=0$ and variance $<[\delta N(\vec{r},z)]^2>=\sigma_N^2(z)$ (the angular brackets $<...>$ stand for statistical averaging). Note that the fluctuations $\delta\varepsilon(\vec{r},z)$ are related to the relative electron density variations $\delta N(\vec{r},z)/N_0(z)$ as:

$$\delta\varepsilon(\vec{r},z)=-[1-\varepsilon_0(z)]\delta N(\vec{r},z)/N_0(z). \qquad (2)$$

Electron density irregularities $\delta N(\vec{r},z)$ (or irregularities in the dielectric permittivity $\delta\varepsilon(\vec{r},z)$) of the magnetized plasma in the upper ionosphere are highly anisotropic, stretched along the geomagnetic field direction $\vec{h}_0$. The position of the unit vector $\vec{h}_0$ in the plane of the geomagnetic meridian $y=0$ (see Figure 1) is specified by the inclination angle I $(-90°\leq I\leq 90°)$, counted from the horizontal plane [Akasofu and Chapman, 1972]. Positive values of I correspond to $\vec{h}_0$

pointing downward (northern hemisphere), while the negative ones correspond to the upward direction (southern hemisphere). Then, for the selected system of coordinates (the x-axis in Figure 3. 1 points to geomagnetic north) we have

$$\vec{h}_0 \equiv \{h_{0x}, h_{0y}, h_{0z}\} = \{\cos I, 0, -\sin I\}. \quad (3)$$

In order to calculate characteristics of scattering of the incident electromagnetic wave by such ionospheric irregularities, let us apply the single scattering approximation method [e.g., Rytov et al., 1987]. In this case it is assumed that $\sqrt{<[\delta\varepsilon(\vec{r}, z)]^2>} << \varepsilon_0(z)$, and therefore, it is possible to ignore the effects of the ionospheric irregularities on the wave trajectories and calculate them within the geometrical optics approximation.

Trajectory parameters of the aspect-sensitive scattered signals. It is known [Gershman et al., 1984] that HF waves incident on the field-aligned irregularities of the upper ionosphere are predominantly scattered in the direction determined by the so-called aspect condition:

$$\vec{K}(z_s) \cdot \vec{h}_0 = 0. \quad (4)$$

Here $\vec{K}(z_s)$ is the scattering vector, which is equal to the difference of the wave vectors of the scattered $\vec{k}^{(s)}(z_s)$ and incident $\vec{k}^{(i)}(z_s)$ fields at the scattering point z_s:

$$\vec{K}(z_s) = \vec{k}^{(s)}(z_s) - \vec{k}^{(i)}(z_s). \quad (5)$$

As is evident from Figure 3.2, equation (4) is satisfied when the angles made by the magnetic field vector with the incident and scattered wave vectors are equal. As a result, the set of vectors $\vec{k}^{(s)}$ forms a characteristic angular cone around the magnetic field with the apex angle ν.

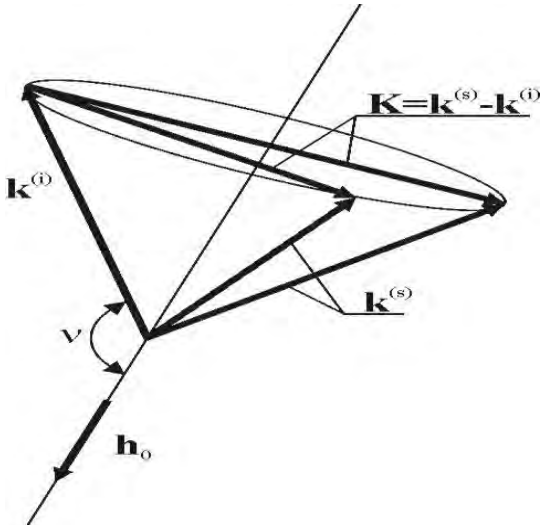

Fig. 3.2. Scattering geometry. Vectors $\vec{k}^{(i)}$ and $\vec{k}^{(s)}$ are, respectively, the incident and scattered wave vectors at the scattering point z_s; $\vec{h}_0$ indicates the direction of the local magnetic field.

In the coordinate system shown in Figure 3.1, and with account of (5), equation (4) can be written as:

$$h_{0x} \cdot (\sin\theta^{(s)} \cos\varphi^{(s)} - \sin\theta^{(i)} \cos\varphi^{(i)}) + h_{0z} \cdot (\cos\theta^{(s)} - \cos\theta^{(i)}) = 0, \quad (6)$$

where $\theta^{(s)}$, $\varphi^{(s)}$ and $\theta^{(i)}$, $\varphi^{(i)}$ are the angles specifying the wave vector positions of the scattered (superscript s) and incident (superscript i) fields at the scattering point z_s (hereafter, symbol z_s is omitted to simplify the equations). Solving equation (6) for $\sin\theta^{(s)}$ and $\cos\theta^{(s)}$, it is possible to derive the direction of the wave vector of the scattered field. Using the relation $\sin^2\theta^{(s)} + \cos^2\theta^{(s)} = 1$, two possible solutions are obtained:

$$\cos\theta_{1,2}^{(s)} = \frac{1}{h_{0z}^2 + h_{0x}^2\cos^2\varphi^{(s)}}\left\{h_{0z}(h_{0x}\sin\theta^{(i)}\cos\varphi_0 + h_{0z}\cos\theta^{(i)}) \pm h_{0x}\cos\varphi^{(s)} \times \right. \tag{7a}$$

$$\left. \times\sqrt{(h_{0x}\cos\theta^{(i)}\cos\varphi_0 - h_{0z}\sin\theta^{(i)})^2 + h_{0x}^2(\cos^2\varphi^{(s)} - \cos^2\varphi_0)}\right\},$$

$$\sin\theta_{1,2}^{(s)} = \frac{1}{h_{0z}^2 + h_{0x}^2\cos^2\varphi^{(s)}}\left\{h_{0x}(h_{0x}\sin\theta^{(i)}\cos\varphi_0 + h_{0z}\cos\theta^{(i)})\cos\varphi^{(s)} \mp \right. \tag{7b}$$

$$\left. \mp h_{0z}\sqrt{(h_{0x}\cos\theta^{(i)}\cos\varphi_0 - h_{0z}\sin\theta^{(i)})^2 + h_{0x}^2(\cos^2\varphi^{(s)} - \cos^2\varphi_0)}\right\}$$

Here the top sign stands for $\theta_1^{(s)}$, while the lower sign stands for $\theta_2^{(s)}$. It is also taken into account that $\varphi^{(i)} = \varphi_0$ according to the equations of geometrical optics for a plane-stratified medium [e.g., Kravtsov and Orlov, 1990]. Note that the incident wave can be scattered either upward ($\cos\theta_{1,2}^{(s)} > 0$), or downward ($\cos\theta_{1,2}^{(s)} \le 0$), i.e., $\theta_{1,2}^{(s)} \in [0,\pi]$. Therefore, the solution space of equation (7) with respect to $\varphi^{(s)}$ is limited by the condition:

$$\sin\theta_{1,2}^{(s)} \ge 0. \tag{8}$$

Another necessary condition for the existence of a real solution of equation (7) is a non-negative argument of the square root in equation (7), i.e.,

$$\cos^2\varphi^{(s)} \ge \cos^2\varphi_0 - \left[\cos\theta^{(i)}\cos\varphi_0 - \frac{h_{0z}}{h_{0x}}\sin\theta^{(i)}\right]^2. \tag{9}$$

The value of $\sin\theta^{(i)}$ at z_s is related to $\sin\theta_0$ at $z = 0$ through Snell's law [Kravtsov and Orlov, 1990]

$$\sin\theta_0 = \sqrt{\varepsilon_0(z)}\sin\theta^{(i)}(z) = \sqrt{\varepsilon_0(z_s)}\sin\theta^{(i)}(z_s). \tag{10}$$

Whence it follows that if $\sin\theta_0 = \sqrt{\varepsilon_0(z)}$ at a certain altitude z, then the value of $\sin\theta^{(i)}$ is equal to 1 at that altitude (i.e., $\theta^{(i)}(z) = \pi/2$). Using equation (1) this condition can also be written as:

$$\omega\cdot\cos\theta_0 = \omega_p(z). \tag{11}$$

Thus, equation (11) determines the critical reflection height z_{cr} for the ray with the incidence angle θ_0 at the lower boundary of the ionospheric layer. This is why when we determine $\cos\theta^{(i)}(z_s)$ two situations are possible, depending on the ratio between $\omega\cos\theta_0$ and ω_{cr} (see Figure 3.3). If $\omega\cos\theta_0 > \omega_{cr}$, then the wave penetrates through the ionospheric layer (no reflection). In this case, within the entire volume of the ionospheric layer with irregularities, the scattering occurs only at the ascending part of the wave trajectory (the direct wave is scattered alone), and the value of $\cos\theta^{(i)}(z_s)$ according to [Kravtsov and Orlov (1990)] is:

$$\cos\theta^{(i)}(z_s) = \sqrt{\cos^2\theta_0 - \omega_p^2(z_s)/\omega^2}. \tag{12}$$

If $\omega\cos\theta_0 \le \omega_{cr}$, then the wave is reflected at $z = z_{cr}$, determined by equation (11), and the range of z_s is limited as $0 \le z_s \le z_{cr}$. As a result, two waves arrive at the scattering point, one being scattered on the ascending part of the trajectory (direct wave), the other on the descending path (reflected wave). Then for $\cos\theta^{(i)}(z_s)$ one gets:

$$\cos\theta^{(i)}(z_s) = \pm\sqrt{\cos^2\theta_0 - \omega_p^2(z_s)/\omega^2}, \tag{13}$$

where "+" and "-" stand for the direct and reflected waves, respectively.

1.

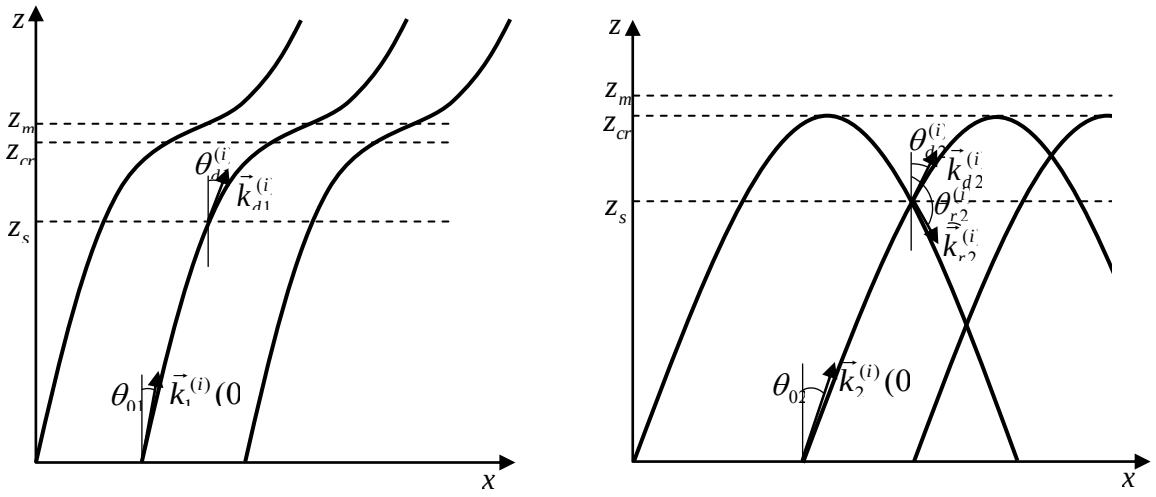

Fig. 3.3. Trajectories of the incident wave for $\omega\cos\theta_0 > \omega_{cr}$ $(\theta_0 = \theta_{01})$ and $\omega\cos\theta_0 < \omega_{cr}$ $(\theta_0 = \theta_{02})$, where ω_{cr} is the critical frequency of the layer (plasma frequency at the height of the layer maximum z_m). In the first case (a), the direct wave $(\theta^{(i)}(z_s) = \theta_{d1}^{(i)})$ alone reaches the scattering height z_s, while in the second case (b) two waves reach the height z_s, specifically, the direct wave $(\theta^{(i)}(z_s) = \theta_{d2}^{(i)})$ and the wave reflected at z_{cr} $(\theta^{(i)}(z_s) = \theta_{r2}^{(i)})$.

Now, consider the scattered wave. Let the background electron density profile $N_0(z)$ be a smooth function with a single maximum $N_m(z_m)$ at z_m (single layer model). If $\omega_{cr} \geq \omega$, then the waves scattered downward $(\cos\theta^{(s)} \leq 0)$ and upward $(\cos\theta^{(s)} > 0)$ both reach the lower boundary of the ionospheric layer at $z = 0$ with an angle $\theta_0^{(s)} \in [\pi/2, \pi]$, which can be found from an equation similar to equation (10), viz.

$$\sin\theta_0^{(s)} = \sqrt{\varepsilon_0(z_s)}\sin\theta^{(s)}(z_s). \qquad (14)$$

If $\omega_{cr} < \omega$, then only the waves scattered at angles $\theta^{(s)}(z_s) \geq \theta_{cr}^{(s)}$ can reach the lower boundary of the ionosphere $(z = 0)$. Here $\theta_{cr}^{(s)} \in [0, \pi/2]$ is a certain critical angle whose value, with account of equation (1) and Snell's law (10), can be determined as:

$$\sin\theta_{cr}^{(s)} = \sqrt{\frac{\omega^2 - \omega_{cr}^2}{\omega^2 - \omega_p^2(z_s)}}. \qquad (15)$$

If $\theta^{(s)}(z_s) < \theta_{cr}^{(s)}$, the scattered wave goes into the upper half-space and then penetrates through the ionosphere. Note that in the case of a multi-layer ionosphere (e.g., E - and F -layers are present) the waves scattered in certain directions can be "trapped" by the interlayer ionospheric waveguide. Such a possibility will be investigated in the next section, but first let us analyze the amplitude characteristics of the aspect-sensitive scattered signals. Scattering cross-section. The effective differential cross-section of a random medium is used to characterize the energy scattered by a unit volume into a unit solid angle in a given direction with a unit flux density of the incident radiation [e.g., Rytov et al., 1987]. In the approximation of a single scattering of electromagnetic waves in random isotropic medium with a regular dielectric permittivity $\varepsilon_0 = const$, the scattering cross section is [Rytov et al., 1987; Gershman et al., 1984]:

$$Q(\vec{K}(z_s)) = P(z_s)\frac{\pi k_0^4}{2}\Phi_\varepsilon(\vec{K}(z_s)) \ . \qquad (16)$$

Here $\Phi_\varepsilon(\vec{K}(z_s))$ is a three-dimensional spatial spectrum of fluctuations $\delta\varepsilon$; $\vec{K}(z_s)$ is the scattering vector given by equation (5); and $P(z_s) = 1 - \left(\frac{\vec{k}^{(s)}(z_s)\vec{e}^{(i)}(z_s)}{k_0\sqrt{\varepsilon_0(z_s)}}\right)^2$ is a polarization factor, where $\vec{e}^{(i)}(z_s)$ is the unit vector of the electric field polarization of the incident wave. Using the same geometrical optics assumptions as in Rytov et al. [1987], it can be shown that equation (16) is applicable to the analysis of the scattering of a single quasi-plane wave in the medium with smooth spatial variations in $\varepsilon_0(z_s)$. The factor $P(z_s)$ is dependent on the incident wave polarization. For instance, according to [Rytov et al., 1987] in the case of a linear polarization

$$P(z_s) = \sin^2\chi(z_s), \qquad (17)$$

and for a circular polarization

$$P(z_s) = \frac{1}{2}(1+\cos^2\gamma(z_s)), \qquad (18)$$

where $\chi(z_s)$ and $\gamma(z_s)$ denote the angles made by the scattered field wave vector $\vec{k}^{(s)}(z_s)$ with the polarization vector $\vec{e}^{(i)}(z_s)$ and wave vector $\vec{k}^{(i)}(z_s)$ of the incident field, respectively.

The anisotropic power law model (e.g., Gershman et al. [1984]) is a conventionally used approximation for the spatial spectrum $\Phi_\varepsilon(\vec{K})$ of the fluctuations $\delta\varepsilon(\vec{r},z)$ in the magnetized plasma of the upper ionosphere for the inertial interval of the wave numbers. In this model, $\Phi_\varepsilon(\vec{K}(z_s))$ can be written as

$$\Phi_\varepsilon(K_{||},K_\perp) = C_\varepsilon^2(z)\left[1+(K_{||}L_{||})^2+(K_\perp L_\perp)^2\right]^{-p/2}, \qquad (19)$$

where $C_\varepsilon^2(z) \sim \sigma_\varepsilon^2(z)$ is a normalization factor, with $\sigma_\varepsilon^2(z)$ representing the variance of the fluctuations $\delta\varepsilon$; $K_{||}$ and $K_\perp$ are longitudinal and transversal (with respect to $\vec{h}_0$) components of the scattering vector $\vec{K}$; $L_{||}$ and $L_\perp$ are characteristic longitudinal and transversal external scale-sizes of the ionospheric turbulence with $L_{||} >> L_\perp$; and $3 < p < 4$.

If condition (4) is satisfied, then equation (16) yields

$$Q(z_s) = P(z_s)\frac{\pi k_0^4}{2}C_\varepsilon^2(z_s)\left[1+K_\perp^2(z_s)L_\perp^2\right]^{-p/2} \ , \qquad (20)$$

where

$$K_\perp^2(z_s) = k_0^2\Big[\sin^2\theta_0^{(s)}+\sin^2\theta_0+(\sin\theta_0^{(s)}\cos\varphi^{(s)}-\sin\theta_0\cos\varphi^{(i)})^2\frac{h_{0x}^2}{h_{0z}^2}- \\ -2\sin\theta_0^{(s)}\sin\theta_0\cos(\varphi^{(i)}-\varphi^{(s)})\Big]. \qquad (21)$$

Equation (21) is inapplicable in the specific case of the horizontal magnetic field, $h_{0z} = 0$, (at the magnetic equator). It can be shown that in this case $K_\perp^2(z_s)$ becomes

$$K_\perp^2(z_s) = k_0^2\left[\sin^2\theta_0^{(s)}+\sin^2\theta_0-2\sin\theta_0^{(s)}\sin\theta_0\cos(\varphi^{(i)}-\varphi^{(s)})\right].$$

Using equation (2), $C_\varepsilon^2(z_s)$ can be expressed as

$$C_\varepsilon^2(z_s) \sim \sigma_\varepsilon^2(z_s) = (1-\varepsilon_0(z_s))^2 \frac{\sigma_N^2(z_s)}{N_0^2(z_s)} = \frac{\omega_p^4(z_s)}{\omega^4} \frac{\sigma_N^2(z_s)}{N_0^2(z_s)}. \qquad (22)$$

Therefore, from equation (20) it is possible to determine the scattering cross-section in the direction defined by the aspect condition (4) for a plane electromagnetic wave propagating in an ionospheric layer with anisotropic electron density irregularities. Note that since $\varphi^{(i)}(z) = \varphi_0$ and $\varphi^{(s)}(z) = \varphi_0^{(s)}$, all the terms in equation (20) can be expressed through the position angles of the incident and scattered field wave vectors at the lower boundary $z = 0$ of the ionospheric layer.

Discussion. As an example, let us first consider scattering of a plane circularly polarized electromagnetic wave propagating vertically in an ionospheric layer with anisotropic irregularities. The wave frequency is assumed to be lower than the critical frequency, $\omega \le \omega_{cr}$. Note that these are typical conditions for the HF heating of the ionosphere.

In a single layer model ionosphere two components will be scattered in the height range $0 \le z_s \le z_{cr}$ (z_{cr} is determined from (11) with $\cos\theta_0 = 1$), which are the direct and reflected waves. Then equation (7) with account of equation (13) yields:

$$\cos\theta_{d,r}^{(s)} = \pm \frac{h_{0z}^2 - h_{0x}^2 \cos^2\varphi^{(s)}}{h_{0z}^2 + h_{0x}^2 \cos^2\varphi^{(s)}}, \qquad (23a)$$

$$\sin\theta_{d,r}^{(s)} = \pm \frac{2h_{0x}h_{0z}\cos\varphi^{(s)}}{h_{0z}^2 + h_{0x}^2 \cos^2\varphi^{(s)}} \ge 0, \qquad (23b)$$

where the "+" and "-" signs stand for the scattering components of the direct (subscript d) and reflected (subscript r) waves, respectively.

As can be seen from equation (23b), in the northern hemisphere ($h_{0x}h_{0z} < 0$) the direct wave is scattered southward ($-90° \le \varphi^{(s)} \le 90°$), while the reflected is scattered northward ($90° \le \varphi^{(s)} \le 270°$). In the southern hemisphere the situation is reversed. Near the magnetic equator ($h_z \approx 0$), as follows from equation (7b), both components are scattered predominantly within the plane perpendicular to the geomagnetic field lines at all angles $\theta^{(s)} \in [0, \pi]$.

To analyze the orientation of the scattered field wave vector at the exit from the ionospheric layer it is convenient to introduce an angle $\theta_{out}^{(s)} = \pi - \theta_0^{(s)}$. Then, according to Snell's law and using equations (23b) and (1), one gets

$$\sin\theta_{out}^{(s)} = \pm \frac{2\sqrt{1-\omega_p^2(z_s)/\omega^2}\, h_{0x}h_{0z}\cos\varphi^{(s)}}{h_{0z}^2 + h_{0x}^2\cos^2\varphi^{(s)}} \ge 0. \qquad (24)$$

As an example, Figure 4 shows isolines for $\varphi^{(s)} = 75°(255°), 45°(225°)$ and $0°(180°)$, which are plotted in the coordinates $\alpha = \omega_p^2(z_s)/\omega^2$ and $\theta_{out}^{(s)}$. The inclination angle I of the geomagnetic field is set equal to $77.5°$ (recall that $h_{0x} = \cos I$ and $h_{0z} = -\sin I$), which corresponds to the location of the EISCAT HF heater ($69°35'$ N, $19°14'$ E). In this case, the wave vector of the scattered component at the lower boundary of the ionosphere ($z = 0$) can be significantly off the vertical despite strongly vertical propagation of the primary wave. The value of this offset increases as α decreases, (i.e., with decrease of the scattering altitude z_s), and/or as the scattering direction approaches the plane of the magnetic meridian. In this example the maximum offset is equal to $\pi - 2I = 25°$, for $z_s = 0$ and $\varphi^{(s)} = 0, \pi$. Analysis of equation (24) shows that such a dependence is valid for the geomagnetic field inclinations $|I| \ge \pi/4$. Otherwise, if $|I| \le \pi/4$, the maximum offset of the aspect-sensitive scattered wave from the vertical,

$\theta_{out}^{(s)} = \pi/2$ (i.e., the scattering within the horizontal plane) will occur for $z_s = 0$ and $\cos\varphi^{(s)} = \pm h_{0z}/h_{0x}$.

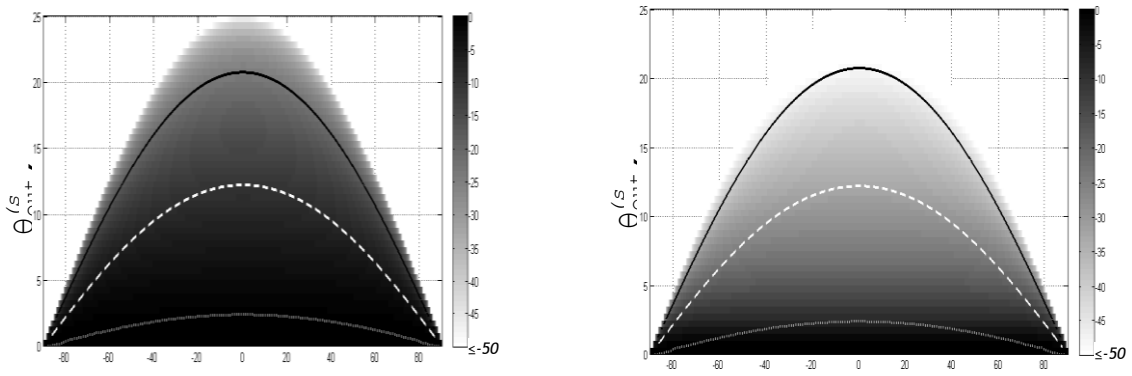

$\varphi^{(s)}$, $\varphi^{(s)}$,
a) b)

Fig. 3. 5. Angular distributions of the value $10\log[Q(z_s)/Q_0(z_s)]$, calculated using equation (25) with $p = 11/3$ for $L_\perp/\lambda_0 = 1$ (a) and $L_\perp/\lambda_0 = 5$ (b). The solid, dashed and dotted lines correspond to the levels $\alpha = \omega_p^2(z_s)/\omega^2 = 0.3$, $\alpha = 0.75$ and $\alpha = 0.99$, respectively. Calculations were made for the vertical incidence at the latitudes corresponding to the EISCAT location ($I = 77.5°$). The value of the scattering cross-section increases with α (i.e., with the scattering height z_s), reaching its maximum at $\alpha = 1$, which corresponds to $\theta_{out}^{(s)} = 0°$.

To calculate the scattering cross section in the direction defined by equations (23) we combine equations (18), (21), and (23) and Snell's law (equation (10)) obtaining for the vertically propagating wave

$$P(z_s) = \frac{h_{0z}^4 + h_{0x}^4 \cos^4\varphi^{(s)}}{(h_{0z}^2 + h_{0x}^2\cos^2\varphi^{(s)})^2},$$

$$K_\perp^2(z_s) = \frac{4k_0^2\varepsilon_0(z_s)h_{0x}^2\cos^2\varphi^{(s)}}{h_{0z}^2 + h_{0x}^2\cos^2\varphi^{(s)}}.$$

Substitution of these expressions together with equation (22) into (20) yields

$$Q(z_s) \sim Q_0(z_s)\frac{\omega_p^4(z_s)}{\omega^4}\frac{h_{0z}^4 + h_{0x}^4\cos^4\varphi^{(s)}}{(h_{0z}^2 + h_{0x}^2\cos^2\varphi^{(s)})^2}\times$$

$$\times\left[1 + \frac{4k_0^2h_{0x}^2L_\perp^2\varepsilon_0(z_s)\cos^2\varphi^{(s)}}{h_{0z}^2 + h_{0x}^2\cos^2\varphi^{(s)}}\right]^{-p/2}, \qquad (25)$$

where $Q_0(z_s) = \frac{\pi k_0^4}{2}\frac{\sigma_N^2(z_s)}{N_0^2(z_s)}$. For quiet ionospheric conditions it is usually assumed that the plasma density fluctuations are proportional to the background electron density, i.e., $\frac{\sigma_N^2(z_s)}{N_0^2(z_s)} = const \equiv \tilde{\sigma}_N^2$. Thus one can write $Q_0(z_s) = \frac{\pi k_0^4}{2}\tilde{\sigma}_N^2$.

Figure 3.5 shows the angular distribution of the value $10\log[Q(z_s)/Q_0(z_s)]$, calculated with equation (25) with $p=11/3$ and $L_\perp/\lambda_0=1$ (top panel), and $L_\perp/\lambda_0=5$ (bottom panel) for the vertical incidence case for the latitude corresponding to the EISCAT location ($I=77.5°$). Here $\lambda_0=f/c=2\pi/k_0$ is the free space wavelength. The results are shown for the scattering of the reflected wave (scattering in the northward direction, $\varphi^{(s)}\in\pm 90°$). For the direct wave (scattering in the southward direction, $\varphi^{(s)}\in 180°\pm 90°$) the angular distributions are completely symmetric. In order to be able to at least roughly relate these data to the scattering heights z_s (or the corresponding plasma frequency $\omega_p(z_s)$) Figure 5 shows isolines for $\alpha=\omega_p^2(z_s)/\omega^2=0.3$ (solid line), $\alpha=0.75$ (dashed line), and $\alpha=0.99$ (dotted line). Note that $\theta_{out}^{(s)}$, $\varphi^{(s)}$ and $\omega_p(z_s)$ are related through equation (24). As is evident from Figure 5, the value of the scattering cross-section increases with α (i.e., with the scattering height z_s), reaching its maximum at $\alpha=1$, which corresponds to $\theta_{out}^{(s)}=0$. This is because $\sigma_N^2(z_s)$ increases with height (since it is assumed that $\sigma_N^2(z_s)\sim N_0^2(z_s)\sim\omega_p^4(z_s)$), and also because the second term in the square brackets of equation (25) gets smaller (since $\varepsilon_0(z_s)\to 0$ as $z_s\to z_{cr}$). The latter effect can be treated as an increase of the signal wavelength in the ionosphere as it approaches the reflection point since $k(z_s)=2\pi/\lambda(z_s)=k_0\sqrt{\varepsilon_0(z_s)}$. Apparently, this is also the reason for the widening of the azimuthal distribution of the scattering cross-section with the decrease of $\theta_{out}^{(s)}$. For example, already for $\theta_{out}^{(s)}\approx 5°\ldots 10°$ the scattering cross–section is practically isotropic in the azimuthal plane, and smaller $L_\perp/\lambda_0$ values lead to greater values of the scattering cross-section. This would suggest that in the presence of several ionospheric layers (e.g., E and F) a certain fraction of the scattered wave energy can be captured by the interlayer ionospheric waveguide. Since such waveguide propagation is characterized by a very small attenuation, it is quite plausible that this mechanism supported the super long distance propagation of the EISCAT signals observed in the "self-scattering" experiment [Zalizovski et al., 2009]. The potential of exciting the ionospheric interlayer waveguide by the aspect-sensitive scattered HF signals requires greater investigation. It should be noted that the role of scattering in HF radio wave trapping into ionosphere waveguides was rather intensively examined as early as in 1970's [e.g., Gurevich et al., 1975; Erukhimov et al., 1975]. However, in contrast to the previous studies, we will be primarily interested in determining the range of θ_0 and φ_0 responsible for channeling scattered signals in a given direction rather than in estimating the trapping coefficient for an incident wave.

Let the ionosphere be represented by two layers, e.g., E and F, each characterized by their respective critical frequencies ω_{crE} and ω_{crF} and critical heights z_{mE} and z_{mF}. We denote the minimum plasma frequency inside the E-F valley at the height z_v as ω_v. Further assume that $\omega_{crF}\geq\omega$, i.e., the wave with frequency ω is reflected from the F-layer (the upper "wall" of the waveguide) at any incidence angle. Obviously, the interlayer waveguide can be excited by the waves scattered in the height range $z_{mE}<z_s<z_{mF}$ only. Therefore, it is necessary for the direct wave to penetrate the E-layer, i.e.,

$$\omega\cos\theta_0>\omega_{crE}. \tag{26}$$

As follows from Snell's law, in order for the scattering component to be confined inside the waveguide, i.e., to be reflected from the E-layer (the lower "wall" of the waveguide), the following condition must be met:

$$\sqrt{\varepsilon_0(z_s)}\sin\theta^{(s)}(z_s)\geq\sqrt{\varepsilon_0(z_{crE})} \tag{27a}$$

which, with account of equation (1), can be recast in a form similar to equation (15):

$$\sin\theta^{(s)}(z_s) \geq \sqrt{\frac{\omega^2 - \omega_{crE}^2}{\omega^2 - \omega_p^2(z_s)}}, \qquad (27b)$$

where $\sin\theta^{(s)}(z_s)$ is determined by equation (7b). Since $\sin\theta^{(s)}(z_s) \leq 1$, it follows from equation (27b) that the scattering should occur within the height range $z_{mE} < z_s < z_F$, where $z_F \in [z_v, z_{mF}]$, and can be determined from $\omega_p(z_F) = \omega_{crE}$.

Further analysis will be carried out for the specific conditions of the "self-scattering" experiment conducted by Zalizovski et al. [2009]. We are primarily interested in the possibility of channeling the EISCAT signals inside the interlayer waveguide in the directions of the receive sites located at UAS, SPB, and RAO. In the chosen coordinate system, $\varphi^{(s)} \approx 135°$ for the UAS station and $\varphi^{(s)} \approx 225°$ for the other two stations. In most heating sessions the EISCAT heater transmitted toward magnetic zenith at one or two close frequencies around 4.04 MHz. The measurements from the collocated ionosonde showed the presence of strong E layers, with the critical frequencies close to and even above the heating frequencies. For the analysis $f_{crE} = 3.9$ MHz and $f_H \approx 1.4$ MHz are assumed and the calculations are not limited to the vertical incidence case, making it possible to investigate the effect of the angles of direct wave incidence. As known [Gurevich, 2007], artificial ionospheric turbulence is effectively produced by the HF heating in the height range with the lower boundary z_{UH}, determined from the upper hybrid resonance condition $f^2 = f_p^2(z_{UH}) + f_H^2(z_{UH})$, where f_H is the gyrofrequency; and the upper boundary z_{cr}, determined by the wave critical reflection condition equation (11). For this reason the plasma frequency $f_p(z_s)$ in the calculations is assumed to vary within the scattering region from $f_p(z_{UH}) = \sqrt{f^2 - f_H^2(z_{UH})} \approx 3.79$ MHz, to $f_p(z_{cr}) = f_{crE} = 3.9$ MHz. Figure 6 shows results of the calculations for such conditions in the system of coordinates with θ_0 (counted radially), and φ_0 (counted counterclockwise). The plots show the distributions of $\sin\theta^{(s)}$ values which satisfy the conditions of excitation of the interlayer ionospheric waveguide (see equation (27b)). The calculations were made for $f = 4.04$ MHz, $\varphi^{(s)} = 135°$ and $f_p = 3.79$ MHz (Figure 6a) and $f_p = 3.87$ MHz (Figure 6c). Figures 6(b) and 6(d) show the respective distributions of the value $10\log[Q(z_s)/Q_0(z_s)]$ for $p = 11/3$ and $L_\perp/\lambda_0 = 1$. The values are given in grayscale (see the legends on the right). As follows from equations (7) and (21), the distributions of $\sin\theta^{(s)}$ for $\varphi^{(s)} = 225°$ will be the same as in Figure 6 (a) and (c), while the distributions of $10\log[Q(z_s)/Q_0(z_s)]$ will look like mirror images of Figure 6 (b) and Figure 6 (d) with the reflection line at $\varphi_0 = 180°$. Note that limits of the region from which the scattered signals are captured by the interlayer waveguide are determined at the level $\sin\theta^{(s)}(z_s) = \sqrt{\frac{\omega^2 - \omega_{crE}^2}{\omega^2 - \omega_p^2(z_s)}}$ (see equation (27b)), which is approximately equal to 0.754 for $f_p = 3.79$ MHz and 0.909 for $f_p = 3.87$ MHz. The dashed line in Figure 6 shows the EISCAT antenna beam at the half-power level. As can be seen, the signal propagation through the interlayer duct channel in the azimuthal directions $\varphi^{(s)} = 135°$ and $\varphi^{(s)} = 225°$ is possible for the given orientation of the heater antenna

only for a very narrow range of angles near $\theta_0 \approx 15°$ and $\varphi_0 = 180°$, with characteristic sizes (for $f_p = 3.87$ MHz) of $\pm 15°$ in azimuth and less than $1°$ in θ_0 (see Figure 3.6 a).

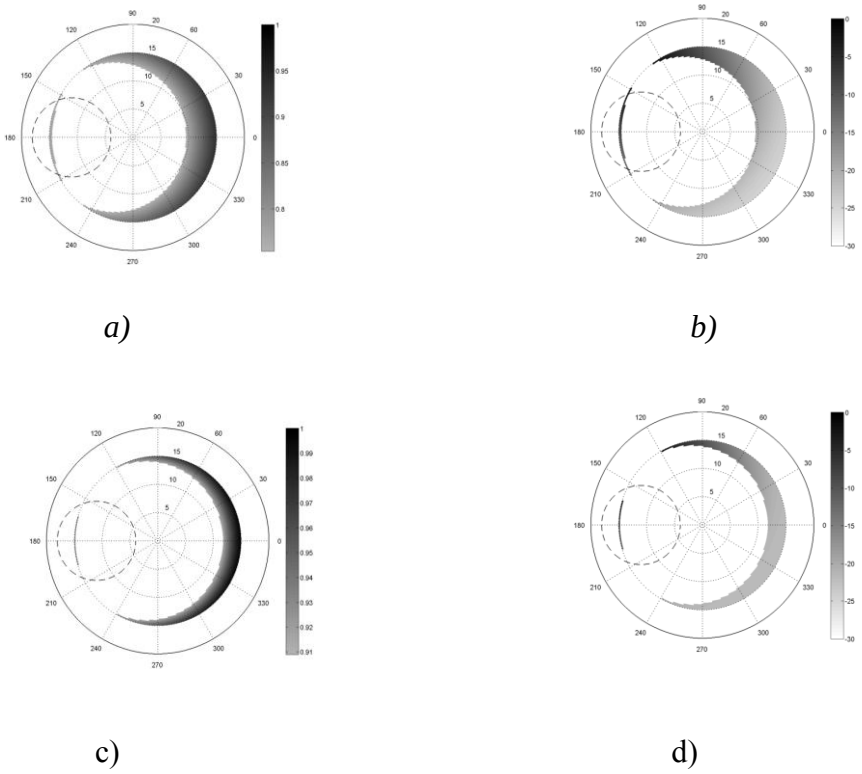

a) *b)*

c) d)

Fig. 3. 6. Distributions of the $\sin\theta^{(s)}$ values which satisfy the condition of excitation of the ionospheric interlayer waveguide (equation (27b)). Calculations were made for $f = 4.04$ MHz, $\varphi^{(s)} = 135°$ and $f_p = 3.79$ MHz (a) and $f_p = 3.87$ MHz (c). Panels (b) and (d) show the respective distributions of the values $10\log[Q(z_s)/Q_0(z_s)]$ for $p = 11/3$ and $L_\perp/\lambda_0 = 1$. The values are shown in grayscale (see legend on the right side) in the coordinate system with θ_0 (shown as radius) and φ_0 (counted counterclockwise). The dashed line shows the EISCAT antenna beam at the half power level. It can be seen that for the given orientation of the heater antenna, signal propagation in the interlayer waveguide toward the receive sites is possible only for a very narrow range of angles near $\theta_0 \approx 15°$ and $\varphi_0 = 180°$, with characteristic sizes (for $f_p = 3.87$ MHz) about $\pm 15°$ in azimuth and less than $1°$ in θ_0.

Accordingly, the linear size of the scattering region at 200 km is approximately 45 to 50 km across and 3 to 4 km along the magnetic meridian. Note that, as follows from equation (7), this case corresponds to the scattering of the ionospherically reflected signal. The sharp cutoff at $\theta_0 \approx 15°$ is determined by condition (26) for the direct wave to penetrate the E-layer. The value of $10\log[Q(z_s)/Q_0(z_s)]$ in this angular range varies insignificantly, from about -4 to -12 (see Figure 3.6 b). As f_p increases, i.e., as the scattering height z_s approaches the critical reflection height z_{cr}, the angular and linear sizes of the scattering region decrease by approximately a factor of 2 (see Figure 3 6 c), while the cross-section changes insignificantly (see Figure 3. 6 d).

The above analysis supports the mechanism of the "self-scattering effect" that was suggested by Zalizovsky et al. [2009] for the explanation of their experimental results of

monitoring the EISCAT transmission at three remote locations (SPB, RAO, and UAS). Recall that during the experiment the variations of the Doppler frequency shifts recorded at all the sites were almost identical. During the experiment significant variations of the electron density were also observed by the EISCAT incoherent scatter radar in the height range from 100 to 200 km. Such variations can significantly affect the Doppler frequency shift and amplitude of the HF heating signal as was demonstrated by the authors using computer modeling. With the above analysis we have demonstrated that the angular sizes of the scattering region responsible for the excitation and subsequent channeling of the HF signals through the interlayer waveguide to the receive sites are rather small (see Figure 3.6). Therefore, it is reasonable to assume that all remotely recorded signals first travel through the same irregularities in the lower ionosphere, and are equally affected by them. Then, the signals reflected from the ionospheric F-layer are scattered by field-aligned irregularities produced by the same EISCAT heating transmission and propagate toward the receive sites through the ionospheric waveguide. Since the scattering region guiding the signals into the interlayer duct channel for propagation into different directions is the same, it is plausible to expect that the variations of the Doppler frequency shifts and signal amplitudes recorded at greatly dispersed receive sites will be very similar, as was observed during the "self-scattering" experiment reported by Zalizovski et al. [2009].

Conclusions. In this chapter the ray optics approximation and small perturbation method were used to analyze the effect of refraction on the scattering characteristics of HF signals scattered by random field-aligned irregularities of the ionospheric plasma. The calculations are carried out for an isotropic plane-stratified (on average) ionosphere, i.e., the incident and scattered waves were both assumed to propagate along unperturbed trajectories. The equation of the so-called aspect-sensitive scattering is derived which relates the trajectory characteristics of the incident and aspect-sensitive scattered waves. The scattering cross-section is calculated within the Born approximation for a plane electromagnetic wave propagating in the ionospheric layer with anisotropic electron density irregularities. For the vertical incidence scenario the intensities of the aspect-sensitive scattered wave (cross-section) and its exit angle are calculated as functions of the scattering direction and height. A possibility of excitation of the interlayer ionospheric waveguide by the aspect-sensitive scattered signals with a selected orientation of the horizontal projection of the wave vector is investigated in dependence on the angles of direct wave incidence. It is demonstrated that such possibility can be implemented using powerful HF heaters, like EISCAT or HAARP. Under certain conditions (e.g., specific orientation of antenna beam), the scattered HF signals can be trapped inside the waveguide and subsequently channeled to very long distances because of the very small attenuation characteristic of the interlayer waveguide.

Thus, the aspect-sensitive scatter mechanism can explain the "self-scattering effect" which was observed using the EISCAT transmission by Zalizovsky et al. [2009]. Therefore, there exists the potential for the practical applications in HF communication, although further studies are required for a more reliable assessment. In particular, it is necessary to consider the suggested mechanism with account of the magnetic field effects which can influence essentially propagation of the incident and scattered waves. Addressing this issue properly would require application of full scale 3D numerical ray-tracing. The authors plan to carry out the respective analysis in the future and present the results in a separate publication. As a first approximation, however, we think that neglecting the geomagnetic field effect on radiowave trajectories is a legitimate approach, which was also taken by other authors [e.g., Gurevich et al., 1975]. The results of this investigation can be useful for the analysis and interpretation of the experiments on HF signals scattering from artificial and natural ionospheric irregularities in the ionosphere, for the development of new methods of diagnostics of the near-Earth plasma turbulence, and also for the investigation of the mechanisms of super-long range propagation of HF electromagnetic emission.

References to Chapters 1- 3

Akasofu, S. I., and S. Chapman (1972), Solar-Terrestrial Physics*, Clarendon Press, Oxford.*

Bezrodny, V. G., P. V. Ponomarenko, and Y. M. Yampolski (1997), Ionospheric scattering of broadcast signals as a source of stochastic interference to highly sensitive HF radio systems, 12-th International Zurich Symposium and Technical Exhibition on Electromagnetic Compatibility*, February 18-29, Zurich, Switzerland, 123-126.*

Bourdillon, A., C. Haldoupis, and J. Dellone (1995), High-frequency Doppler radar observations of magnetic aspect irregularities in the midlatitude E region ionosphere, J. Geophys. Res.*,* 100*, 21503-21521, doi:10.1029/95JA01079.*

Djuth, F. T., B. W. Reinisch, D. F. Kitrosser, J. H. Elder, A. Lee Snyder, and G. S. Sales, Imaging HF-Induced irregularities above HAARP, Geophys. Res. Lett.*, 33(4), L04107, doi:10.1029/2005GL024536, 2006.*

Erukhimov, L. M., S. N. Matyugin, and V. P. Uryadov (1975), Radio-wave propagation in an ionospheric wave channel, Radiophysics and quantum electronics*, 18(9), 958-963, doi: 10.1007/BF01038191.*

Galushko, V. G., A. V. Koloskov, V. V. Paznukhov, B. W. Reinisch, G. S. Sales, Y. M. Yampolski, and A. V. Zalizovsky (2008), Self-scattering of the HF heater emissions observed at geographically dispersed receiving sites, Antennas and Propagation Magazine, IEEE*,* 50*, 155-161.*

Gershman, B. N., L. M. Erukhimov, V. Yu. Kim, V. P. Uryadov, and E. E. Tsedilina (1975), Influence of scattering on radio-wave trapping in ionospheric waveducts, Radiophysics and quantum electronics*, 18(9), 964-972, doi: 10.1007/BF01038192.*

Gershman, B. N., L. M. Erukhimov, and Yu. Ya. Yashin (1984), Wave Processes in Ionosphere and Space Plasma*, Nauka, Moscow, (in Russian).*

Gurevich, A. V. (2007), Nonlinear phenomena in the ionosphere, PHYS-USP*,* 50*, 1091-1121.*

Hysell, D. L. (2008), 30 MHz radar observations of artificial E *region field-aligned plasma irregularities,* Annales Geophysicae*,* 26*, 117-129.*

Koloskov, A. V., T. B. Leyser, Yu. M. Yampolski, and V. S. Beley (2002), HF pump-induced large scale radial drift of small scale magnetic field-aligned density striations, J. Geophys. Res.*,* 107*, 1097, doi:10.1029/2001JA000154.*

Kravtsov, Yu. A., and Yu. I. Orlov (1990), Geometrical optics of inhomogeneous media*, Springer-Verlag, Berlin; New York.*

Lyon, G. F. (1965), The anisotropy of ionospheric irregularities deduced from VHF scatter measurements, J. Atmos. Terr. Phys.*,* 27*, 1213-1216.*

Myasnikov, E. N., N. V. Muravieva, E. N. Sergeev et al. (2001), Spatial spectrum of the artificial ionospheric disturbances induced by powerful HF radiowaves. Radiophysics and Quantum Electronics*,* 44*, 833-846.*

Rytov, S. M., Kravtsov, Yu. A. , and Tatarskii, V. I., Principles of Statistical Radiophysics*, Vol. I-IV, Berlin, Springer-Verlag, 1987.*

Zalizovski, A. V., S. B. Kashcheyev, Y. M. Yampolski, V. G. Galushko, V. S. Belyey, B. Isham, M. T. Rietveld, C. La Hoz, A. Brekke, N. F. Blagoveshchenskaya, and V. A. Kornienko (2009),
Self-scattering of a powerful HF radio wave on stimulated ionospheric turbulence, Radio Science*,* 44*, RS3010, doi: 10.1029/2008RS004111, 1-12.*

Yampolski, Y. M., V. S. Beley, S. B. Kasheev, A. V. Koloskov, V. G. Somov, D. L. Hysel, B. Isham, and M. C. Kelley (1997), Bistatic HF radar diagnostics of induced field-aligned irregularities, J. Geophys. Res.*,* 102*, 7461-7468.*

4. Studies of the Ionospheric Turbulence Excited by the Fourth Gyroharmonic at HAARP and ionospheric wave guide excitation

There are the results of experiments conducted during the HAARP BRIOCHE June 2014 campaign, whose objective was to study the development of artificial ionospheric turbulence. During the experiments, the heating frequency was stepped up near the 4th gyroharmonic, and the power of the heating HF radiation was varied. Our diagnostics included: measurements of phase-derived Slant Total Electron Content using the L1/L2 GPS signals received at HAARP; measurements of Stimulated Electromagnetic Emission (SEE) conducted 15 km away from the HAARP site; ionograms from HAARP's digisonde and reflectance data from Kodiak radar; and detection of the HAARP HF radiation scattered into the ionospheric channel and propagated for 15.6 Mm to the receiver at Antarctica Peninsula.

Additionally, a new method of diagnostic was introduced during this campaign. This method was developed of the IRA NASU team in a frame of the EOARD – STCU Partner Project P-524. HAARP radiated HF waves can be scattered into the ionospheric waveguide by artificial irregularities, and can propagate along the waveguide like a sound wave in the whispering gallery mode. The waveguide was oriented along the Earth's terminator which was passing over the transmitting and receiving sites simultaneously. Furthermore the electron density gradients formed in the ionosphere when the terminator's passage occurs near the receiving site could scatter the HF signals from the waveguide to the groundbased receiver. We were able to detect the scattering HAARP signals on the ground at Ukranian Antarctic Station (UAS) (coordinates 65.25 S, 64.25 W) at 15.6 Mm from HAARP. The HF signals were recorded within frequency band 500 Hz centered at the carrier frequency of the HAARP pumped signal. The data acquisition system collected records of the intensity and the Doppler spectra of the signal with time resolution 1 sec and 5 sec. This paper introduces a successful attempt to use the effect of long distance HF propagation for diagnostic of the artificial turbulence. Finally, all the experiments were diagnosed by the iononosonde, and by the Kodiak coherent radar located 670 km South West from HAARP.

Ionospheric conditions. The two experiments discussed were conducted during 20 minutes each starting at about 3 UT, i.e around 7 p.m. local time. During the first day (06/06/14) the ionosphere was slightly disturbed (δB~50 nT); a noticeable sporadic E-layer existed (f_0E_s~4.5 MHz); f_OF_2 was in the frequency range 5.6-5.7 MHz while the F2 peak was located at h_mF_2=270 km. Considering the oblique propagation of the heating wave, its frequency was reflected from the F2 peak thus, for the majority of the experiment, the heating wave was strongly absorbed in the ionosphere due to anomalous absorption. An exception was the time around 3:04 UT when the ionogram revealed that f_OF_2 dropped below 5.4 MHz, thus the heating frequency exceeds the critical frequency, and the ionosphere became transparent to the HF wave.

During the second day (06/07/14) the ionosphere was also quiet (δB~30 nT) with E_s layer present. However, the ionosphere was unstable, half of the ionograms reveal that f_OF_2 fell to 4.05-4.5 MHz, thus the HF frequency was higher than the critical frequency and absorption was low and the artificial turbulence was almost absent, while the rest of the ionograms show f_OF_2>5.7 MHz and h_mF_2=270km, and thus at the time the artificial turbulence was pumped. Note that due to the experiment restrictions the minimum heating frequency was 5.67 MHz which was above the 4th gyro resonance. In our March 2013 experiment [Najmi et al., 2014] we have obtained the resonance frequency 5.76 MHz from the SEE spectrum, at which frequency, the DM disappeared. The ionogram shows that 5.76 MHz waves are reflected at 190 km.

An estimate based on the dipole model of the geomagnetic field shows that in the June 2014 experiments the 4th gyro resonance occurs at 5.6 MHz, $4 f_{ce} = 5.76MHz\left(\frac{R_E + 190km}{R_E + 250km}\right)^3$, where 250 km is the reflection height of 5.6 MHz taken from ionograms. Thus the lowest heating frequency 5.76 MHz is close to the BUM cutoff which is about 8 kHz above the 4th gyroharmonic, i.e. at 5.68 MHz [Leyser et al., 1994].

SEE observations. Stimulated Electromagnetic Emission (SEE) signals were measured simultaneously with the STEC using an HF detector operated by the Naval Research Laboratory 15 km away from the HAARP site. Figure 4.1 shows the power spectral density (PSD) of the SEE emission for each of four chosen heating frequencies, 5.67, 5.70, 5.73 and 5.76 MHz, which reveal distinct BUM. At higher heating frequencies BUM disappears. The traces are averaged over a 10s portion of the heating period with constant ERP. The heating frequency is shown by the highest peak in the center at Δ_F=0, the down shifted maximum (DM) is on the left side of the heating frequency at Δ_F=-10 kHz, while the broad upshifted maximum (BUM) is on the right side of the plots in the range of Δ_F=+30-130 kHz. In each of the panels of Fig. 4.1, the blue trace corresponds to the power 2.5 kW, green to 5.0 kW and red to 10 kW per transmitter (the power level 25, 50, and 100% respectively). Note that the shape of SEE signal saturates at the half full power. Figure 5a,b shows the amplitude of the PSDs normalized by its peak values as a function of heating power. Here Fig. 4.2 a) corresponds to the BUM amplitude while Fig. 4.2 b) shows the evolution of the DM amplitude. In those two cases saturation at 90% level occurs at about ½ of the full power.

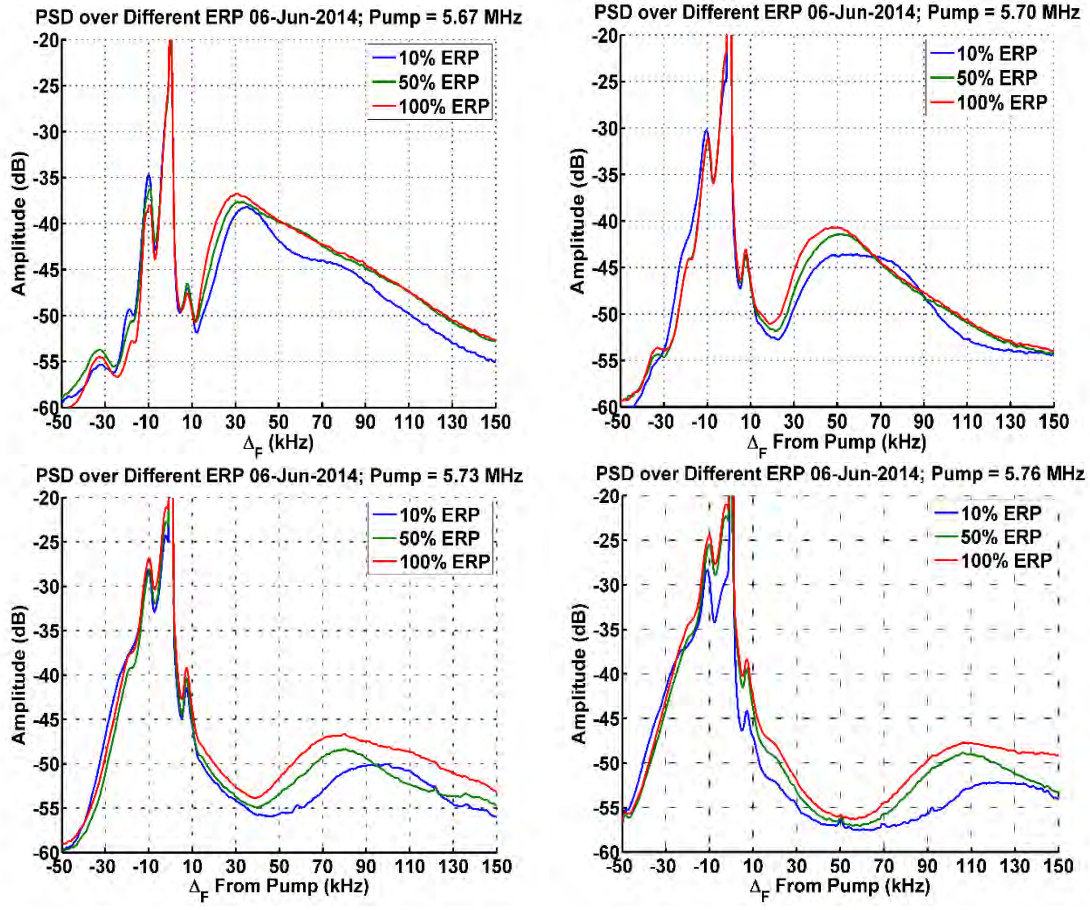

Fig. 4.1. Power spectral density (PSD) of the SEE emission for each of four chosen heating frequencies, 5.67, 5.70, 5.73 and 5.76 MHz, which reveal distinct BUM.

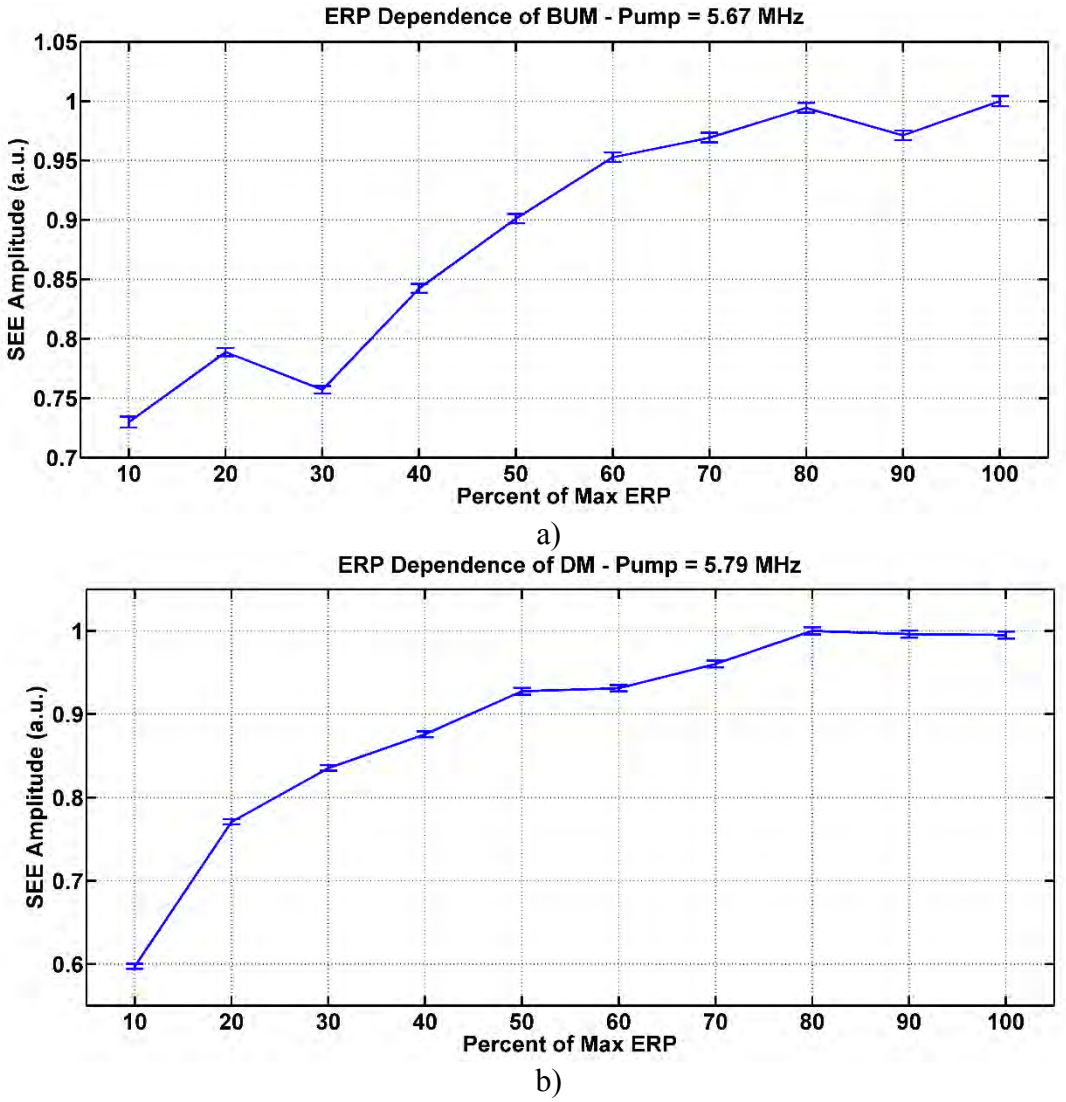

Fig. 4.2. Behavior of the BUM amplitude.

Observations made by the Kodiak radar. Figure 4.3 a) plots time series of the SNR of reflected as detected by the Kodiak radar. We chose beam 9 directed towards HAARP's heated region, the frequency of the probing signal is about 12 MHz. The signal reflected by the artificial ionospheric turbulence is centered at 700 km slant range. During the 10th cycle at 03:12:00-03:14:30, the SNR was strongly reduced since Kodiak's beam 09 was almost out of the HF heating spot. This was a geometric effect of the angular adjustments of the beam to track PRN 25 and this final heating cycle was picked up by beam 10. The HF heating was switched on at 02:55 followed by the buildup of the reflected radar signal over 25 sec. Then a strong SNR of more than 50 dB was detected.The reflection increases by ~10 dB around 02:57 then it dips around 03:00 and 03:04 due to the decrease in the ionospheric plasma density. The second dip was reflected in the ionogram as discussed above, while the first dip occurred during the time not covered by the ionograms at HAARP. Between 03:11:30 and 03:13:30 the SNR decreases, at 03:14:30 the heater was switched off and the reflection gradually disappeared.

Figure 4.3 b) shows time series of the velocity of the ionospheric irregularities. Starting at 02:55:00, the irregularities quickly accelerate to 35-40 m/s, peak at ~60 m/s near 02:57:00-02:59:00, then gradually reduce to ~30 m/s.

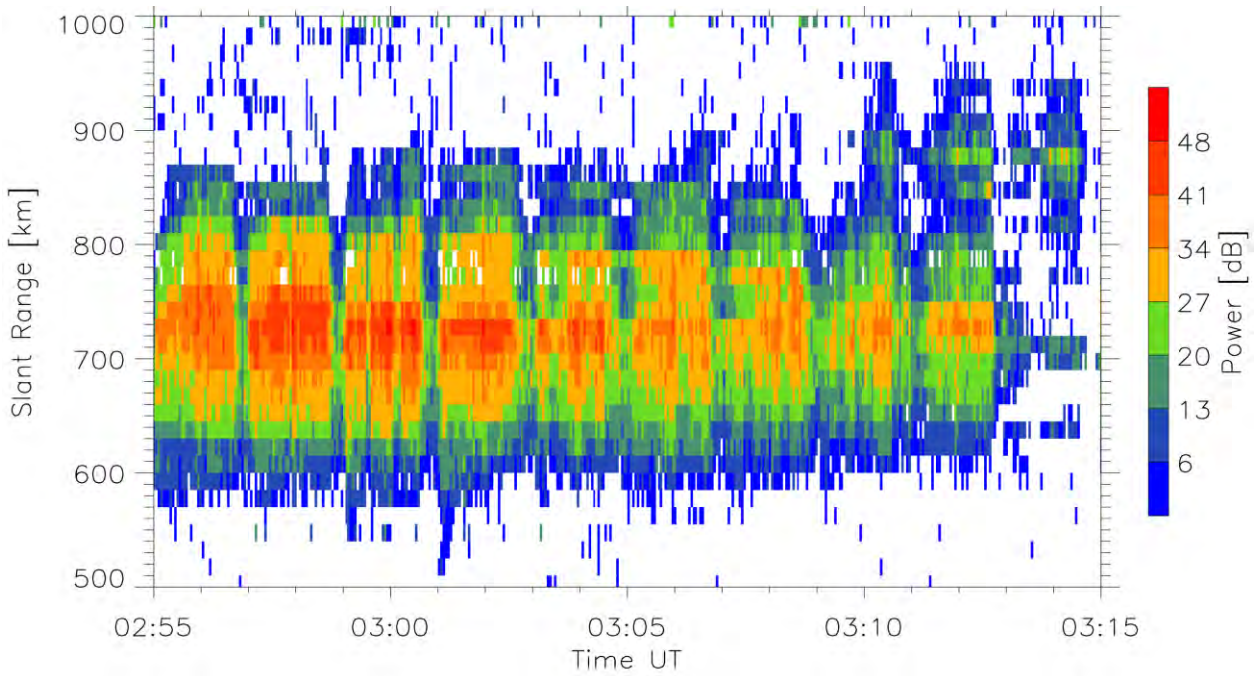

a)

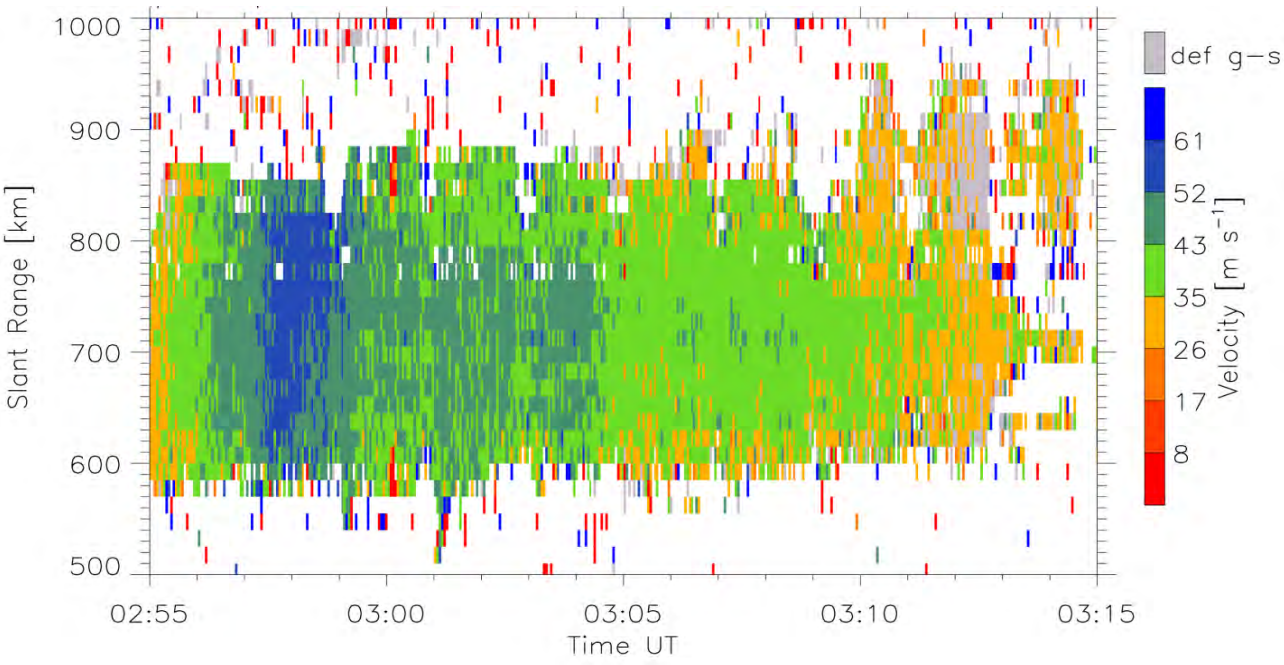

b)

Fig. 4.3. Kodiak radar observations

HAARP signals detected at UAS. Monitoring of the HAARP HF signals was carried out at the Ukrainian Antarctic Station (UAS) "Academik Vernadsky". Figures 4.4 a) and 4.4 b) show the spectrogram of the detected signal for June 6 and 7, 2014, while figure 4.5 shows the intensity of the detected signal on June 6th.

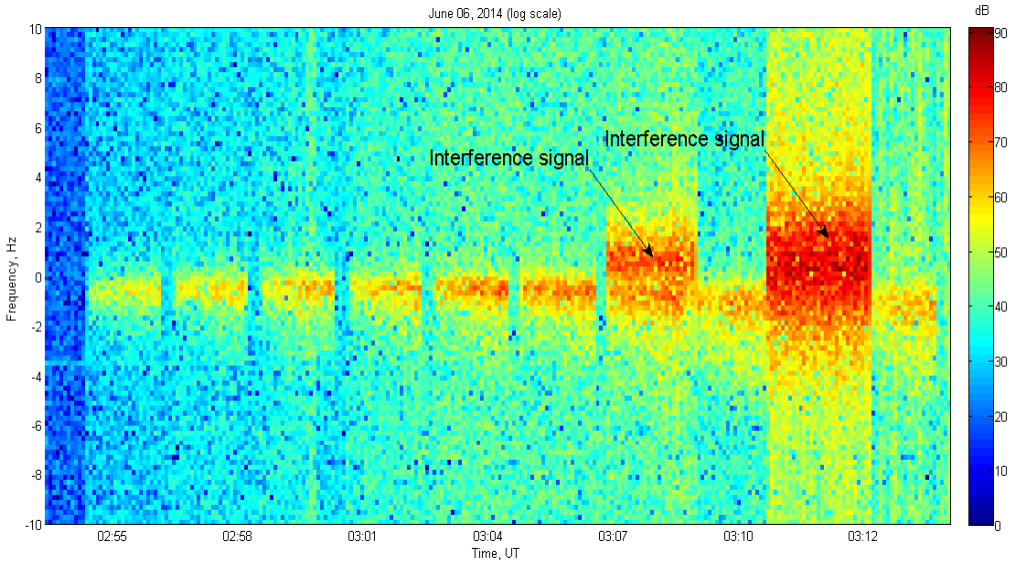

a)

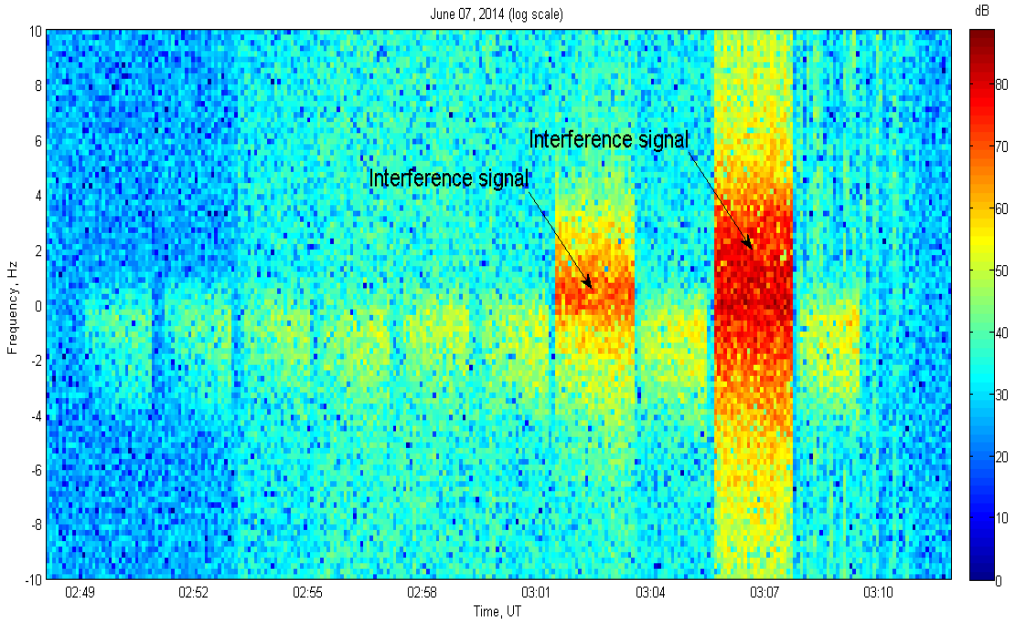

b)

Fig. 4.4. Spectrograms as detected in Antarctica at the "Akademik Vernadsky" station for June 6 (a) and 7 (b).

The 8-th (f_h = 5850 kHz) and 9-th (f_h = 5910 kHz) heating cycles, indicated by black arrows at the spectrograms, were contaminated by interference signals and therefore were not processed in Fig. 4.6 which reveals the signal-to-noise ratio of the signals intensity. Figure 4.5 shows that the intensity of detected signal strongly depends on the heating frequency f_h. In fact, for f_h slightly

above the 4th gyro the intensity of the detected signal was very low, hardly above the noise level. The intensity of the detected signal went up with f_h and peaks at 5.79 MHz.

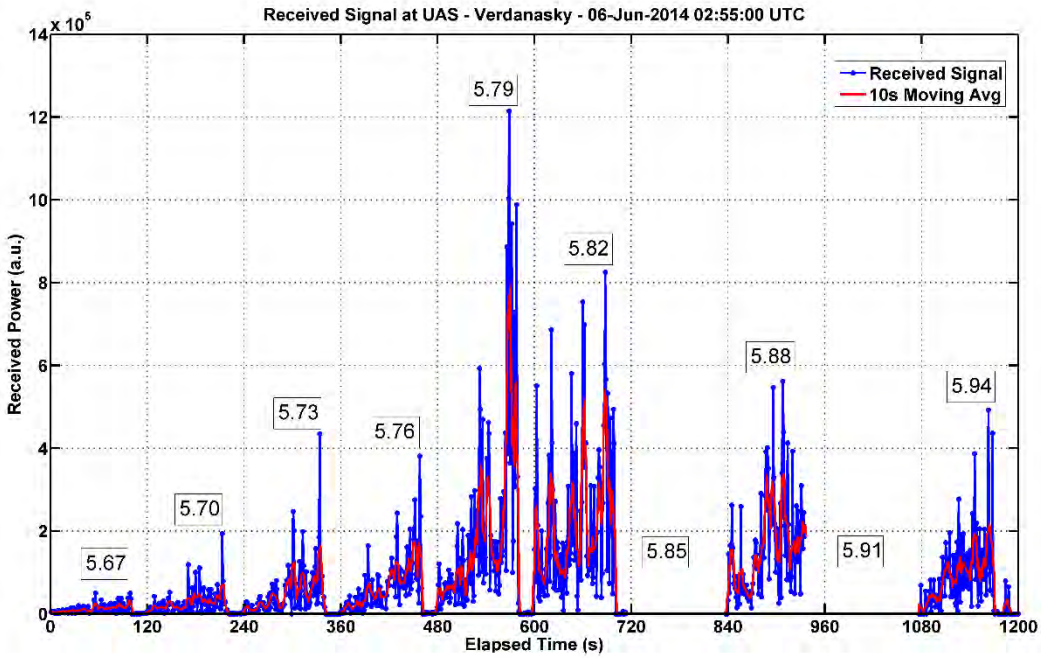

Fig.4.5. Frequency dependency of the detected signal intensity.

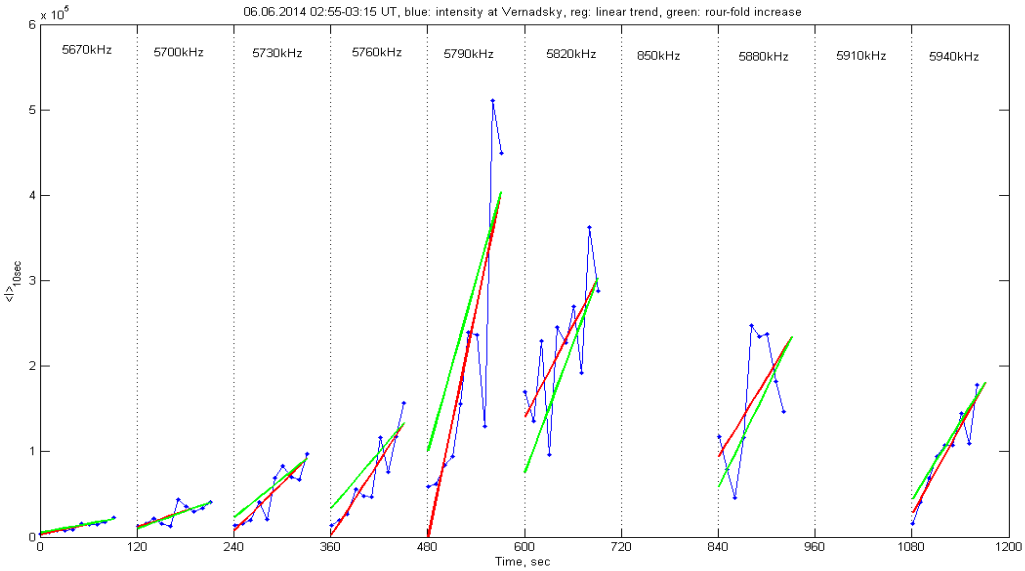

Fig. 4.6. Signal to noise ratio.

Further, Fig. 4.6 shows how the signal changes with the intensity of the HAARP heater at the different heating frequencies (the blue lines). The green lines correspond to 4 times increase of the heating power, the linear interpolation is shown by the red lines in both Fig. 6. Similar results were obtained on June 7 except that the signal-to-noise ratio was by 5-10 dB less than that on June 6 (see Fig. 4.4 a and Fig. 4.4. b).

The spectral width as a function of the heating frequency is shown in Fig.4.7 for each of 100 s time interval which correspond to the heating by a chosen frequency.

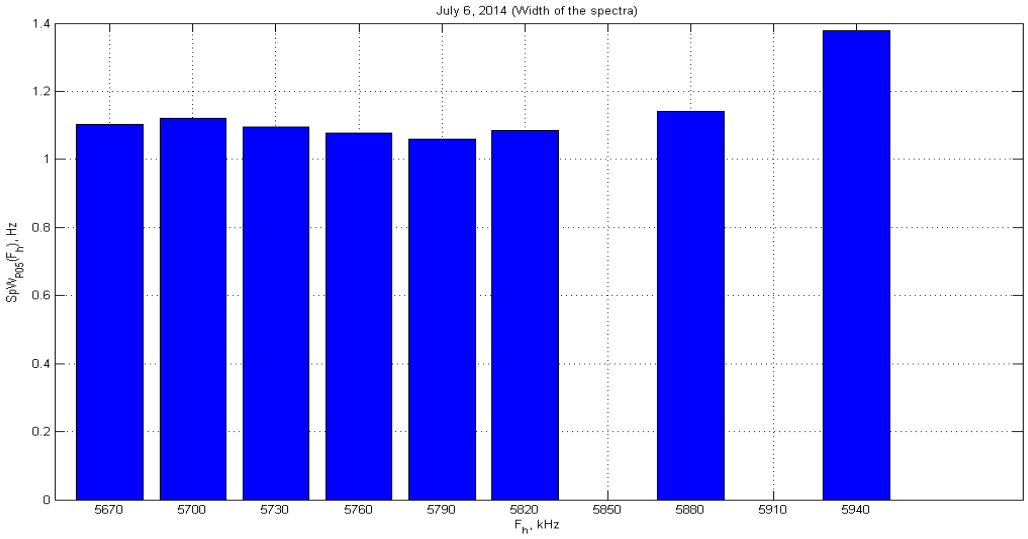

Fig. 4.7. Spectral width of the signals detected in Antarctica.

The spectral width at half power was obtained by using smoothed spectral curves. It was found that the narrow spectral width was about 1 Hz on 6/6/2014 and increase to 2 Hz at 6/7/2014.
Finally we obtain the S_4 scintillation index over 100 s time interval as above. It is presented in Fig. 4.8. as a function of the heating frequency for June 6 and 7 experiments.

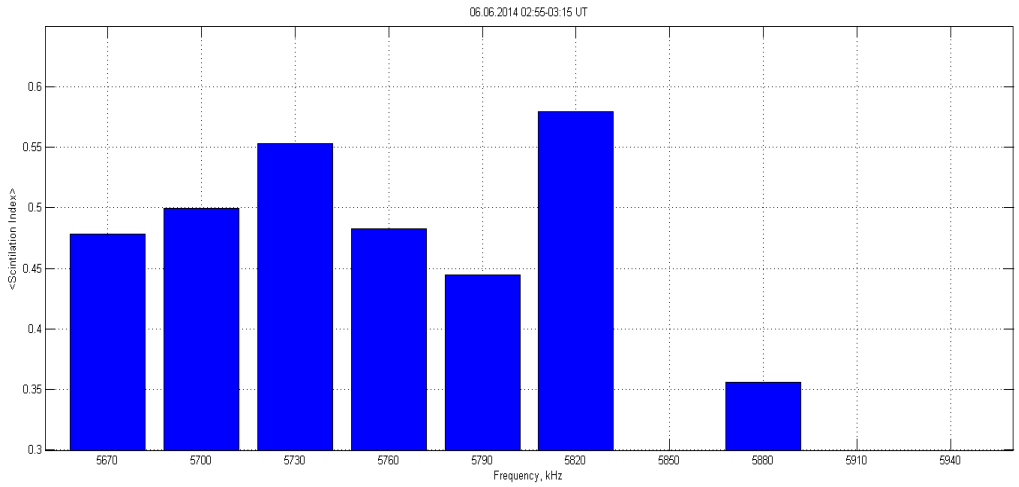

Fig.4.8. S_4 scintillation index of intensity of the detected HAARP signals.

In both experiments the S_4 index peaked at f_h=5.73 MHz i.e. when the SSS, indicated by the BUM, begin to be suppressed by the long scale striations such as revealed by the DM, the latter effectively scatter the HF waves.

Discussion . Now we discuss the probing of the AIT by HAARP HF waves scattered by the AIT into the ionospheric waveguide. The radio waves were detected and processed at Ukrainian Antarctic Station (UAS) 15.6 Mm away from HAARP. The results of these experiments were presented in Section 3, here we analyze the related physical processes. Note that Zalizovski et al. [2009] detected HF signals from EISCAT facility at Ukrainian Antarctic Station (UAS) located 16.3 Mm from the heater. The HF signal revealed two different components, one a narrowband "mirror-reflected" and another "scattered" having a few times wider spectrum. It was mentioned by Zalizovski that although both components propagate along the ionospheric channel the mirror-reflected signal is associated with the side lobe radiation of the transmitting HF antenna, which bypasses the modified volume, while the scattered signal was radiated through the main antenna beam and then scattered by pump-induced plasma striations. Notice that in order to distinguish which of the two mechanisms dominates one needs to sweep the heating frequency around the multiple gyro resonance. While the sidelobe radiation is not sensitive to the frequency variations, the spectrum of the pumped striations, so, the scattered signal strongly depends on the f_h choice.

Figure 4.9 shows amplitudes of PSDs obtained from the SEE spectrum combined with the intensity of the HAARP signal measured at UAS taken from the Doppler spectrum (Fig.4.4) versus the heating frequency.

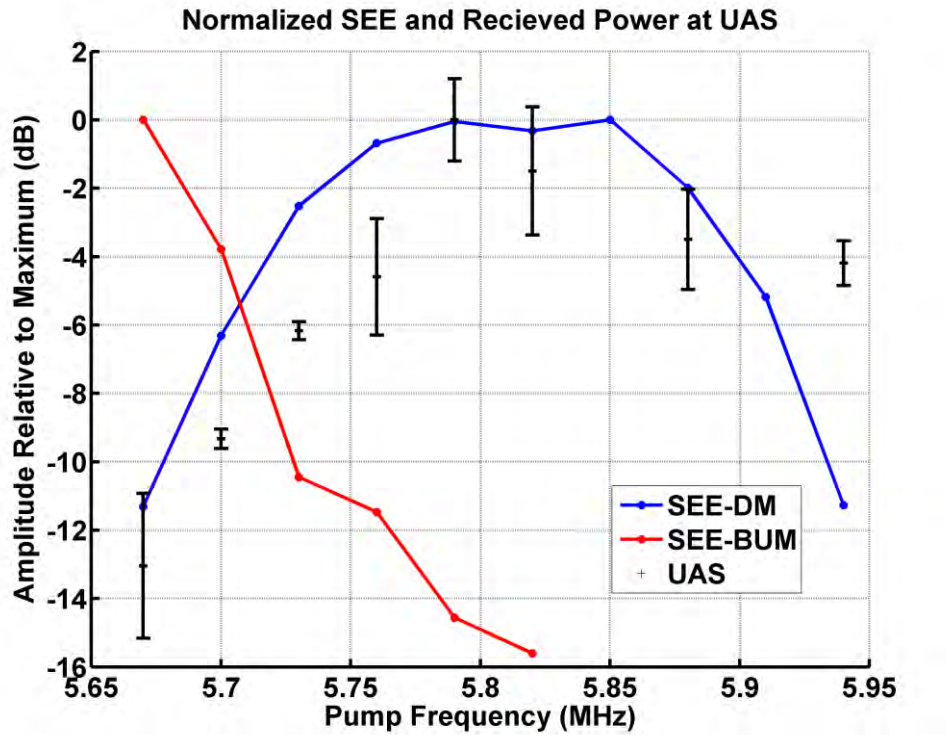

Fig.4.9. Amplitudes of PSDs of SEE and intensity of the HAARP signal measured at UAS.

The red and blue lines in Fig 4.9 show the amplitude of the BUM and DM respectively, both normalized by their peak values. The black line shows the intensity of the detected HAARP signal first smoothed by moving average (red trace in Fig 4.5) and then normalized by its peak value.

Note that the Doppler broadening detected on June 6th reveals that Δf_D=1.15-1.40 Hz. This corresponds to the velocity of ionospheric irregularities $v = \frac{c\Delta f_D}{2 f_h} = 30 - 35$ m/s, and it is consistent with the velocity found by Kodiak in figure 4.3. It was found that the intensity of the signal detected at UAS during the experiments on June 6 and 7 strongly depends on the heating frequency f_h. Figure 9 reveals that on 06/06 when the BUM is dominant in the SEE spectrum it suppresses the HF signal. The stronger is BUM the weaker is the HF signal. To the contrary, when the DM dominates in the SEE spectrum intensity of the detected signal went up with f_h and peaks at 5.79 MHz. Thus the DM and HF peaks occur at the same frequency.

Furthermore, it is known that the BUM is associated with the pumping of 10 cm transverse scale striations, often called super small striations (SSS), while the DM is associated with the 7-30 m scale striations [Norin et al., 2008]. Since SSS inefficiently scatter the HF waves compared to the decameter striations related to the DM, this implies that the HAARP signal detected at UAS could be due to the scattering of the HF radiation having the half wavelength of 25 m by the decameter size artificial striations into the ionospheric channel.

The analysis shows that origin of the detected signal at the "Akademik Vernadsky" station is scattering of the HAARP's HF radiation off of artificially pumped striations and into the ionospheric waveguide. In this process, mirror reflection does not appear to play an important role, as indicated by the low amplitude of received signal at 5.67 and 5.70 MHz. Since the amplitude of the signal varied nonlinearly with the HF power at 5.76, 5.79 and 5.82 MHz, the signal cannot be induced by sidelobe radiation which is known to be linear in the radiated power. Still the question remains why the observed spectrum is relatively narrow about 1-2 Hz width, which is similar to that observed by Zelizovski et al. [2009] of the mirror-reflected signal component while the scattered signal was much broader up to 10-20 Hz.

References to Chapters 4

Bernhardt, P.A., C.A. Selcher, R.H. Lehmberg, S. Rodriguez, J. Thomason, M. McCarrick, G. Frazer (2009), Determination of the electron temperature in the modified ionosphere over HAARP using HF pumped stimulated Brillouin scatter (SBS) emission lines, Annales Geophysicae, 27, 4409-4427.

Bernhardt, P.A., C.A. Selcher, S. Kowtha (2011), Electron and ion Bernstein waves excited in the ionosphere by high power EM waves at the second harmonic of the electron cyclotron frequency, Geophys. Res. Lett., 38, L19107, doi:10.1029/2011GL049390.

Carozzi, T.D., B. Thide, S.M. Grach, T.B. Leyser, M. Holz, G.P. Komrakov, V.L. Frolov, E.N. Sergeev (2002), Stimulated electromagnetic emissions during pump frequency sweep through fourth electron cyclotron harmonic, J. Geophys. Res., 107(A9), 1253, doi:10.1029/2001JA005082.

Frolov, V., M. Erukhimov, S.A. Metelev, E.N. Sergeev (1997), Temporal behavior of artificial small-scale ionospheric irregularities: Review of experimental results, J. Atmos. Solar-Terr. Physics, 59, 18, 2317-2333.

Galushko, V. G., A. V. Koloskov, V. V. Paznukhov, B. W. Reinisch, G. S. Sales, Y. M. Yampolski, and A. V. Zalizovsky (2008), Self-scattering of the HF heater emissions observed at geographically dispersed receiving sites, Antennas and Propagation Magazine, IEEE, 50, *155-161.*

Gurevich, A.V., K.P. Zybin (2006), Strong field aligned scattering of UHF radio waves in ionospheric modification, Phys. Lett. A., 358, 159-165, doi:10.1016/j.physleta.2006.05.064.

Huang, J., S.P. Kuo (1994), A theoretical model for the broad upshifted maximum in the stimulated electromagnetic emission spectrum, J. Geophys. Res., 99, A10, 19569-19576.

Kotov, P. V., E. N. Sergeev, S. M. Grach (2008), Spectra of stimulated electromagnetic emission of the ionosphere upon sweeping of the pump wave frequency near gyroharmonics. Experimental results, Radiophys Quantum Electronic, 51, 417-430, doi: 10.1007/s11141-008-9043-5.

Leyser, T.B., B. Thide, H. Derblom, A. Hedberg, B. Lundborg, P. Stubbe, H. Kopka (1989), Stimulated electromagnetic emission near electron cyclotron harmonics in the ionosphere, Phys. Rev. Lett., 63,11.

Leyser, T.B., B. Thide, M. Waldenvik, S. Goodman, V.L. Frolov, S.M. Grach, A.N. Krashtin, G.P. Komrakov, D.S. Kotik (1993), Spectral structure of stimulated electromagnetic emissions between electron cyclotron harmonics, J. Geophys. Res., 98, A10, 17595-17606.

Leyser, T.B., B. Thide, M. Waldenvik, E. Veszelei, V.L. Frolov, S.M. Grach, G.P. Komrakov (1994), Downshifted maximum features in stimulated electromagnetic emission spectra, J. Geophys. Res., 99, A10, 19555-19568.

Mahmoudian, A., W.A. Scales, P.A. Bernhardt, B. Isham, E. Kendall, S.J. Briczinski, N.E.B. Fuentes, O. Vega-Cancel (2014), Electron gyro-harmonic effects on ionospheric stimulated brillouin scatter, Geophys. Rev. Lett., doi:10.1002/2014GL06105U.

Najmi, A.C., G. Milikh, J. Secan, K. Chiang, M. Psiaki, P. Bernhardt, S. Briczinski, C. Siefring, C.L. Chang, K. Papadopoulos (2014), Generation and detection of super small striations by F region HF heating, J. Geophys. Res. Space Physics, 119, doi:10.1002/2014JA020038.

Norin, L., S.M. Grach, T.B. Leyser, B. Thide, E.N. Sergeev, M. Berlin (2008), Ionospheric plasma density irregularities measured by stimulated electromagnetic emission, J. Geophys. Res., 113, A09314, doi:10.1029/2008JA013338.

Norin, L., T.B. Leyser, E. Nordblad, B. Thide (2009), Unprecedentedly strong and narrow electromagnetic emissions stimulated by HF radio waves in the ionosphere, Phys. Rev. Lett., 102, 065003, doi: 10.1103/PhysRevLett.102.065003.

Ponomarenko, P.V., T.B. Leyser, B. Thide (1999), New electron gyroharmonic effects in the HF scatter from pump-excited, field-aligned ionospheric irregularities, J. Geophys. Res., 104A, 10081-10087, doi: 10.1029/1999JA900039.

Thide, B., E.N. Sergeev, S.M. Grach, T.B. Leyser, T.D. Carozzi (2005), Competition between Langmuir and upper hybrid turbulence in an HF pumped ionosphere, Phys. Rev. Lett., 95, 25, doi: 10.1103/PhysRevLett.95.255002.

Zalizovski, A.V., S.B. Kashcheyev, Y.M. Yampolski, V.G. Galushko, V. Belyey, B. Isham, M.T. Rietveld, C. La Hoz, A. Brekke, N.F. Blagoveshchenskaya, A. Kornienko (2009), Self-scattering of a powerful HF radio wave on stimulated ionospheric turbulence, Radio Science, 44, RS3010, doi:10.1029/2008RS004111.

5. Conclusions

The Project was aimed at experimentally investigating the possibility of exciting the ionospheric interlayer duct channel using powerful radiations from the heaters HAARP (Alaska, USA) and EISCAT (Tromsø, Norway), as well as from HF broadcasting stations RWM (Moscow, Russia) and CHU (Ottawa, Canada). Major attention was paid to analyzing the possibility of exciting the interlayer ionospheric waveguide which support super-long range HF propagation with a small amount of attenuation. To monitor the radiation a compact-size receiving complex was developed which is capable of measuring the signal intensity and spectral characteristics in an off-line automatic mode. Two facilities of the kind have been constructed in the course of the Project fulfillment. One of these was deployed in Ukraine at the Low-frequency Observatory of the IRA NASU (Martova village, Kharkov region) in 2012, while another was installed at the Ukrainian Antarctic station "Akademik Vernadsky" in the Antarctic in 2013. In addition, similar receiving complexes were involved during the Project-related measuring campaigns, which had been constructed by the Project participants under other research projects and put into operation in the Northern Scandinavia (Tromso, Norway), on the Svalbard Island (Spitsbergen Archipelago) and Equatorial Africa (Lagos, Nigeria). Such a chain of the receiving and transmitting sites made it possible to simultaneously investigate probe signal propagation along radio paths of various lengths, specifically, quasi-vertical (less than 100 km), middle (up to 3000 km) and super-long range (from 10000 to 16000 km). In all, about 100 hours have been spent for observations of the radiation from powerful heaters (mostly, of the EISCAT heater) and more than 3000 hours for monitoring signals from broadcast radios. In a number of cases the signal strengthening was detected for the super-long range radio links (Alaska-Antarctica and Northern Scandinavia-Antarctica) which effect can be regarded as a result of the waveguide propagation. To explain the mechanisms of the waveguide excitation and extraction of the radio wave energy from it, the effect of aspect-sensitive scattering of signals by natural and artificial field-aligned irregularities of the ionospheric plasma was considered as the basic one. A pioneering feature of the developed theoretical model is the account of the regular ionospheric refraction. The aspect-sensitive contours in the ionosphere and on the Earth's surface have been calculated for all the transmitting and receiving sites for the current ionospheric conditions. During the measurement campaigns with the use of radiations from the powerful heaters two other effects have been occasionally revealed, which are the combination (Brillouin) signal scattering by the artificially stimulated plasma turbulence and excitation of the second harmonic of the powerful radiation in the HF-modified ionosphere. As planned, a software package has been developed for the remote control of the receiving complexes and visual representation of the measurement results in real-time through the internet. It should be noted that throughout 2013 the HAARP heater was out of operation because of the lack of the operational cost. In view of this, all the measurement campaigns on monitoring the powerful transmitter signals in the Antarctic have been carried out using the EISCAT heater under conditions which were not always optimum for the ionospheric waveguide excitation. For the same reason the receiving complex for the Antarctic has been provisionally deployed at the Ukrainian Antarctic station "Akademik Vernadsky". The most fruitful experiments were performed in a frame of BRIOCHE heating campaign in June 2014. The detail description of this campaign is included in the Final Report (Chapter 4). All results the previous EISCAT heating campaigns were included into the Interim Project report.

The results obtained during the Project fulfillment have been published in fours scientific papers and reported at several international meetings in the USA, Puerto-Rico and Ukraine.

IRA Project team would like to thank Dr. G. Milikh from Departments of Physics and Astronomy, University of Maryland, College Park, MD who provided our participation in the BRIOCHE heating campaign.